Synthesis of carbon dioxide hydrates in a slurry bubble column

By

Denis Myre

Thesis submitted to the Faculty of Graduate and Postdoctoral Studies in Partial Fulfillment of the Requirements for the Degree of M.A.Sc in Chemical Engineering

Department of Chemical and Biological Engineering
University of Ottawa
February 2011

Statement of Contribution of Collaborators

I declare that I am the sole author of this thesis. The heat transfer experiments with the three-phase inverse fluidized bed and the synthesis of carbon dioxide hydrates in the high-pressure slurry bubble column were performed by me. Discussions with Dr. Phillip Servio (Chemical Engineering Department, McGill University) were helpful in the interpretation of results in Chapter 3.

My supervisor, Dr. Arturo Macchi, of the Department of Chemical and Biological Engineering, University of Ottawa supervised my work during the M.A.Sc. program and provided editorial corrections.

Signature:_____ Date:_____

Abstract

Carbon dioxide hydrates were synthesized in a 0.10m I.D. and 1.22m tall bubble column equipped with a cooling jacket for heat removal. Visual observations at different driving forces (pressures between 2.75 and 3.60 MPa and temperatures between 0 and 8ºC) were recorded with a digital camera through a sight glass of 118.8 by 15.6 mm. The superficial gas velocity was varied from 20 to 50 mm/s to attain different levels of turbulence in the liquid. The growth rate was found to be dependent on the sequence/method used to reach the operating temperature and pressure. A greater supersaturation was obtained when the system temperature and pressure were reached with very low or no bubble-induced mixing. As a result, hydrates nucleated and grew immediately when starting the gas flow with the reactor volume being quickly filled with hydrates. Moreover, the hydrate growth rate and solution final density were higher when operating conditions partially condensed CO_2 resulting in greater interphase mass transfer rates. In parallel, since hydrate formation is an exothermic process and the reaction is often limited by the rate of heat removal, heat transfer measurements were achieved in a simulated hydrate environment. The instantaneous heat transfer coefficient and related statistics gave insight on the role of bubbles on heat transfer and hydrodynamics.

Sommaire

Dans cette étude, nous avons synthétisé des hydrates de dioxyde de carbone dans une colonne à bulle ayant un diamètre interne de 0,10 m et une hauteur de 1,22 m, et munie d'une chemise de refroidissement pour évacuer la chaleur. À l'aide d'une caméra digitale, des observations visuelles ont été enregistrées à différentes forces motrices (la pression variant entre 2,75 et 3,60 MPa et la température entre 0 et 8°C), au travers d'une fenêtre d'observation de 111,8 mm par 15,6 mm. La vitesse superficielle du gaz a été variée entre 20 et 50 mm/s afin d'obtenir différents niveaux de turbulence dans le liquide. Nous avons remarqué que le taux de croissance des hydrates était dépendant de la séquence/méthode utilisée pour atteindre les conditions voulues de température et de pression. Un degré de sursaturation plus élevé a été obtenu lorsque la température et la pression désirées étaient atteintes à très bas mixage ou sans mixage induit par les bulles. Par conséquent, la nucléation et la croissance d'hydrates ont été immédiates lorsque nous avons redémarré le gaz, et le réacteur s'est rapidement rempli d'hydrates. De plus, le taux de croissance des hydrates et la densité finale de la solution étaient plus grands lorsque les conditions d'opération permettaient une condensation partielle du CO_2 résultant en des taux de transfert de matière plus élevés entre les différentes phases. En parallèle, puisque la formation d'hydrates est exothermique et que la réaction est souvent limitée par le taux d'évacuation de la chaleur, des mesures de transfert de chaleur ont été effectuées dans un environnement simulant les hydrates. Des mesures de coefficients de transfert de chaleur instantanés et des statistiques étant reliées ont permis de mieux comprendre le rôle des bulles sur le transfert de chaleur ainsi que sur les phénomènes hydrodynamiques.

Remerciements

Je tiens à remercier sincèrement Dr. Arturo Macchi pour m'avoir donné l'opportunité de travailler sur ce projet. Je le remercie également pour le soutien et la confiance qu'il m'a donnés tout au long de la maîtrise.

Je remercie également Dr. Phillip Servio du Département de Génie Chimique à l'Université McGill pour ces commentaires utiles sur la synthèse d'hydrates.

Je remercie les gens du Département de Génie Chimique et Biologique qui m'ont permis de réaliser les expériences en laboratoire, particulièrement Louis G. Tremblay, Franco Ziroldo, Gérard Nina, et mon collègue et ami Dominic Pjontek.

Finalement, je remercie mon épouse Josianne ainsi que ma famille et mes amis pour le soutien qu'ils m'ont apporté tout au long de mes études.

Table of contents

List of Figures

List of Tables

Chapter 1 - Introduction

1.1 Description of gas hydrates

Gas hydrates are member of the class of compounds labelled "clathrates". They are non-stoichiometric ice-like compounds composed of water and gas molecules. Under certain thermodynamic conditions, hydrogen bonding between water molecules forms a network that includes cavities (or cages) in which gas molecules (guest molecules) can be trapped. This structure occurs at temperature slightly above the freezing point of water and is stabilized by the presence of the guest molecules (Sloan et al., 2008).

The size of the guest molecule determines the water lattice structure. The three most common structures for gas hydrates are structure I (sI), structure II (sII) and structure H (sH). These arrangements differ in their number of cages of various sizes. Table 1 summarize some characteristics of the hydrate structures (Sloan et al., 2008).

Table 1.1: Structure and cage types of the common hydrate structures.

Structure	sI	sII	sH
Crystal group	Cubic	Cubic	Hexagonal
Ideal unit cell formula	$6(5^{12}6^{2})\cdot 2(5^{12})\cdot 46H_2O$	$8(5^{12}6^{4})\cdot 16(5^{12})\cdot 136H_2O$	$1(5^{12}6^{8})\cdot 3(5^{12})\cdot 2(4^{3}5^{6}6^{3})\cdot 34H_2O$
Average cavity radius (Å)	Small cavity=3.95 Large cavity=4.33	Small cavity=3.91 Large cavity=4.73	Small cavity=3.94 Medium cavity=4.04 Large cavity=5.79

For example, hydrates of methane are made of sI unit cells, each consisting of 2 small cages (pentagonal dodecahedron 5^{12} – 12 pentagonal faces with equal edge lengths and equal angles) and 6 larges cages (tetrakaidecahedron $5^{12}6^2$ – 12 pentagonal and 2 hexagonal faces). A unit cell of sI involves 46 water molecules and fits into a 12 Å cube. On the other hand, propane hydrates are built from sII unit cells which consist of 16 small cages (pentagonal dodecahedron 5^{12} – 12 pentagonal faces with equal edge lengths and equal angle) and 8 larges cages (tetrakaidecahedron $5^{12}6^4$ – 12 pentagonal and 4 hexagonal faces). A unit cell of sII involves 136 water molecules and fits into a 17.3 Å cube. Finally, larger guest molecule such as methylcyclohexane in the presence of methane will form sH unit cells which are composed of three different sizes of cages involving 34 molecules of water (Sloan et al., 2008). Structure sI, sII and sH are illustrated in Figure 1.1 (Koh et al., 2007).

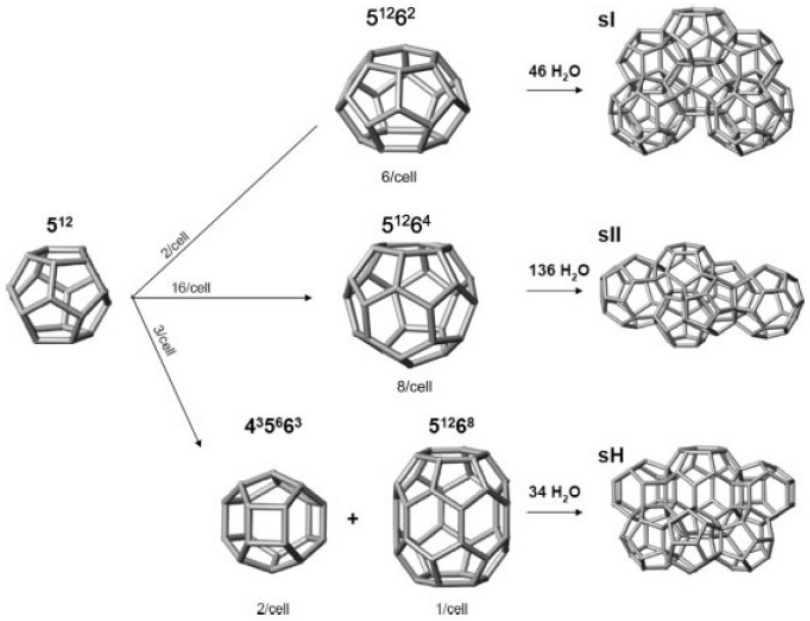

Figure 1.1: Polyhedral water cavities comprising sI, sII and sH hydrates (Koh et al., 2007)

Generally, each cavity of these structures will contain a maximum of one guest molecule. The cage filling depends on pressure, temperature and the nature of the entrapped molecules. The relative water/guest ratio is known as the hydration number. The real hydration number is always higher the ideal hydration number since the cages are rarely all occupied. For example, methane hydrate is typically formed with only 96% of the cages occupied by methane (80-90% of the small cages and 95-99% of the large cages) (Koh et al., 2007). This explains why hydrates are non-stoichiometric clathrate compounds. The hydrate formation is prevented if the guest molecule can establish hydrogen bond since it would make the unit cell structure unstable. Also, a gas molecule that is too small (<3.5 Å) will not be able to stabilize the small cages, while a gas molecule that is too large (>7 Å) will not fit in the large cage cavities. A unit cell structure will be stable only if the large cages can be filled. As an example, since both the small cages (3.95 Å) and large cages (4.33 Å) of a sI unit cell structure can receive a molecule of methane, the structure will be stable. The stabilization of the cages of the different structures depends on the size ratio (i.e. guest diameter/cavity diameter). The size ratios of the guest molecules dictate the crystal structure of the hydrate which in turn determines the equilibrium pressures and temperature for the hydrate phase. The transition to a structure that is more stable involves a lower pressure required to achieve this structure (Sloan et al., 2008). A mixture of gas can also form hydrates in presence of water. Natural gas which contains larger molecules like propane and iso-butane form structure sII by stabilizing the larger cages, while the vacant small cages can be filled by carbon dioxide and methane. One must be prudent when predicting the structure of hydrates, since even though both methane and ethane usually form hydrate with sI structure, their combination can lead to sII structure depending on pressure and composition due to an increase in stability (Koh et al., 2007).

Hydrates are often seen as a problem in gas and oil production and transportation, particularly in subsea flow lines where temperature and pressure are favourable for hydrate to occur. Hydrate forming in flow line may result in blockages, which evidently involves economic lost but also ecological and safety risks. This is why inhibitors are currently used in the industry to prevent blockage and research is still being performed in that domain (Koh et al., 2007). Under certain concentrations, thermodynamic inhibitors such as methanol and glycols prevent the formation of hydrate by establishing hydrogen bonds with water molecules. Salts such as sodium chloride can also be used to prevent the formation of hydrate by the action of their ions interacting with the dipoles of the water molecules, causing the water being attracted more to ions than being attracted to hydrate. Kinetics inhibition using low molecular weight polymer can also prevent the formation of hydrate by bonding the hydrate surface delaying the growth for a period longer that the free water residence time in a pipeline (Sloan et al., 2008).

But the interest in gas hydrates has significantly increased since the early 1990s in the areas of energy and environment (Koh et al., 2007). First, hydrate mainly composed of methane naturally occurs (formed from bacterial methanogenesis or from thermogenic oil and gas reservoir under the sea floor) in the permafrost zone and in sub-sea sediments where the thermodynamic conditions are favourable, i.e relatively high pressure and low temperature. Moreover, their quantity is immense and widely distributed around the globe (Sloan et al., 2008). As a result, methane hydrates are seen as a potential energy resource. Many studies have focused in determining the total amount of hydrates in the world. In 2008, this quantity of methane in hydrates was estimated to be in the order of 10^{15} to 10^{18} sm^3, i.e. around 10 times the amount of conventional natural gas (CCA, 2008). Canada benefits from being

surrounded by oceans as its gas hydrate reserve would be in the order of 10^{12} to 10^{14} sm^3. Again, this is potentially 10 fold to the Canada's estimated potential of conventional natural gas in 2004 ($14.2x10^{12}$ m^3). However, further research and explorations are still needed to access the quantity of hydrates and the reservoirs quality in Coasts and Arctic region (CCA, 2008). In USA, it is estimated that gas from hydrates represents 300 times the quantity of the total remaining recoverable conventional reserves (Koh et al., 2007). Furthermore, in the context of climate change, methane hydrates in the permafrost may dissociate and methane being release in the atmosphere, engendering a snowball effect since it is an efficient greenhouse gas (Koh et al., 2007). Consequently, it may be worthwhile to use its energy and transform it into CO_2 which is more than twenty times less effective in trapping heat in the atmosphere than methane (http://www.epa.gov/methane/). Up to now, production of methane from natural gas hydrates is still more costly compared to conventional natural gas reservoir. However, the decline in reserves of conventional gas resources added to the research being conducted in technologies for lowering exploitation costs will make the natural gas hydrates option more appealing over time, particularly in regions where these conventional gas sources do not exist, in reducing both transportation costs and risk of supply (CCA, 2008).

Another field of interest is the capture of carbon dioxide under its hydrate form and its sequestration in the deep ocean in order to reduce the emission of this greenhouse gases in the atmosphere (Aaron et al., 2005; Kang et al., 2000). Although carbon dioxide hydrates is expected to be unstable in seawater, the release rate is much smaller than other methods including injection of liquid CO_2 drops (hydrates sinks while CO_2 droplet rises and dissolution rate of liquid CO_2 is greater than dissolution of hydrates) (Lee et al., 2003). However, converting carbon dioxide into hydrates from post-combustion gas requires

relatively high pressure (~70bar at 273K) because of the presence of nitrogen in a large proportion (only ~17% of CO_2) (Kang et al., 2000). Alternatively, recovering CO_2 from rich source (i.e. synthesis gas) involves higher proportion of carbon dioxide (~40% CO_2, 60% H_2), consequently requiring lower pressure (Linga et al, 2010; Yang et al., 2008). In both case, the addition of hydrate promoters such as tetra-n-butyl ammonium bromide, tetra-n-butyl ammonium fluoride, THF, propane, H_2S, which can be used to induce the formation of different hydrates structure at lower pressures to reduce operating costs (Aaron et al., 2005; Fan et al., 2009; Li et al, 2009, Linga et al, 2010; Kang et al., 2000). For example, the equilibrium hydrate formation pressure for a gas composition of 17 mol% CO_2 and 83% N_2 is shifted from 83.5 bar to 4.75 bar at 275 K when THF is added to the aqueous solution in a proportion of 1 mol % (Kang et al., 2000). This technology would not be more energy intensive than other methods (Chemical absorption, pressure swing adsorption, etc.) and benefits from having a product that is easier for transport than CO_2 gas (Aaron et al., 2005).

Sequestration of CO_2 in deep oceans in replacement of methane during energy production from natural gas hydrate deposits is also considered. But the effectiveness of this strategy is controversial and needs further investigation. In fact, the dissociation rate of carbon dioxide hydrates in the sea floor has been found to be significantly higher than for methane hydrates due to the higher solubility in water of CO_2 compared to CH_4 (Koh et al., 2007).

1.2 Interest for gas hydrates for transportation and storage of gas

Hydrates are also seen a potential avenue for transportation and storage of natural gas and hydrogen. Currently, methods for natural gas exportation includes: pipelines, liquefied natural gas (LNG), compressed natural gas (CNG), gas-to-liquid (GtL). In addition to

requiring high pressure (45-76 atm), involving expensive cost for pipe installation (1-5 million/mile) and demanding compressor stations, pipelines suffers from being limited to only one general destination. On the other hand, liquefied natural gas requires temperature of -162°C at 1 atm, and contains 637 Sm^3 gas per m^3. However, this method requires installation of large scale refrigeration units, and consequently it is not economically attractive for locations where the resource is far from the demand, as well as locations where the reserve is small. Compressed natural gas has typically pressures between 120 and 250 atm, depending on its composition, and contains about 200 Sm^3 gas per m^3. These high operating pressures involve immense capital cost for compressors, and also imply large operating and maintenance costs. Natural gas can also be converted into liquid hydrocarbons in gasification and reforming processes and subsequent Fisher-Tropsch reactions. Afterward, liquid hydrocarbons can be transported under less intensive conditions compared to natural gas (Thomas et al., 2003).

Alternatively, natural gas could be transported/stored under its hydrate form. Natural gas hydrates occurs between 8-10 MPa and 2-10°C, and contains 160 Sm^3 gas per m^3. Once synthetized, they can be stored and transported under less intensive conditions (i.e. 0°C at 10 atm, or -10°C at 1 atm) (Thomas et al., 2003). Furthermore, the dissociation rate is potentially limited by a self-preservation characteristic of hydrates that is function of pressure, temperature and gas content. It is thought that the formation of a thin layer of ice on the hydrate pellets would significantly reduce the liberation of hydrate former gas molecules. The best condition for self-preservation was found to be 0.3 MPa and -4°C (Giavarini et al., 2004). The relatively less severe conditions required for formation and storage of natural gas hydrates compared to conventional methods, added to the possibility of exploiting small

reserve for which utilisation of conventional methods would not economically viable justify the research being conducted in the development/improvement of natural gas hydrate processes.

Furthermore, economic analysis of capital costs has been performed to compare the whole chain of production and transport NGH and LNG. The study considers on-land production, sea-transport by tankers and on-land regasification. It was found that initial costs for NGH could be lower than LNG of the same scale by a factor up to 25% (Gudmundsson et al., 1996; Kanada et al., 2006).

In 2005, Mitsui was producing 600 kg/day of NGH in a demonstration plant as the first-stage Process Development Unit in a continuously sparged stirred tank reactor operated at 5.5 MPa and 277 K. In their Bench Scale Unit, they included a dehydration unit that allowed to increases the hydrate content (by removing a proportion of water not used for in hydrates but present in the slurry) from 10 to 40% m^3 hydrate/m^3 vessel. A pelletizing/granulating unit was expected to increase the hydrate content to 75% vol. in 2008. The pelletized/granulated hydrate spheres are more stable and are easy handling (Watanabe et al., 2008). Mitsui is planning to commercialize their process in 2012-2013 with an expected capacity of 6000 ton/day (Iwasaki et al., 2005). If the feasibility study proves the capacity of the technology, NGHJ (natural gas hydrate Japan) will work to supply 10 million metric ton/year (LNG equivalent) of natural gas to global consumers in 2020-2030 (http://www.mes.co.jp/english/business/energy/energy_09.html).

1.3 Technologies for hydrate formation

The assessment of the potential of hydrates as an alternative for gas transportation and storage involves many study fields, including the production, pelletizing, transportation, and degasification. In this work, we are only focussing on methods of production, since research is still needed to find an efficient reactor for hydrate production (Linga et al., 2010).

Processes being studied for hydrate production include systems having either the gas or water as the dispersed phase. The processes can also be semi-batch wise or continuous. The different options will be discussed in this section.

1.3.1 System of gas hydrate formation with liquid water as the dispersed phase

For systems having the liquid as the dispersed phase, water is sprayed at the top of the reactor which contain the gas. The pressure is controlled by the amount of gas in the reactor, while temperature is controlled by the means of a heat exchanger in the water circulation loop. A pump is required to recirculate the fluid. In its semi-continuous mode, the hydrates are accumulating in the system, while in the continuous mode, hydrate slurry is continuously removed. In that case, additional water is fed to the water circulation loop. Figure 1.2a illustrates such systems in the semi-continuous mode. This kind of process was exploited by many researchers (Kobayashi et al., 2007; Murakami et al., 2009; Fujita et al., 2009; Matsuda et al., 2006).

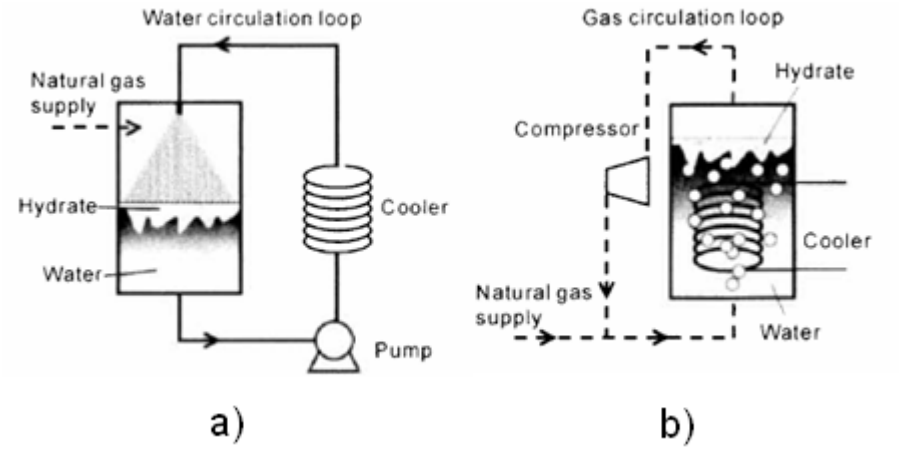

Figure 1.2: Illustration of hydrate forming systems operating in semi-continuous mode (Mori, 2003).

The main advantage of those systems is the high gas/water interfacial area that is increased by atomizing the liquid water. Moreover, the high translational velocity of water droplet eliminates the requirement of mechanical agitation. However, those systems suffer from the poor removal of heat of hydrate formation through the wall because of the low heat capacity of the gas and the low convective transport of heat. Also, the quantity of hydrates produced is limited to a slurry solution in order to avoid the obstruction of the water circulation loop by the hydrates (Mori, 2003).

1.3.2 System of gas hydrate formation with gas as the dispersed phase

For systems having the gas as the dispersed phase, the gas is fed through the bottom of the reactor which contains the liquid water. The pressure is controlled by the gas in excess at the top of the reactor which acts as a piston. Temperature is controlled by the means of cooling jacket or a coil. For such system, a compressor can be used to recirculate the excess gas. In its semi-continuous mode, the hydrates are accumulating in the system, while in the continuous mode, hydrate slurry is continuously removed. In that case, additional cooled

water is continuously fed to the reactor. Figure 1.2b illustrates such system in the semi-continuous mode. This kind of reactor was exploited by Luo et al. (2007).

The main advantage of those systems is the large proportion of water (high heat capacity) and the convection caused by the rising gas bubble, allowing an efficient removal of heat of reaction through the reactor wall. Also, in the semi-batch mode, it is possible to completely convert the water into a dry powdery solid of hydrate. This form can be useful for a further pelletizing process. A disadvantage is the need for the recirculation of the excess gas that involves additional costs. However, this loop can be omitted if the gas bubbles are small enough to completely react during their rise in the water pool. Some reactors include a stirrer to increase the interfacial area between water and gas (Lee et al., 2005; Linga et al., 2010; Mork et al., 2002; Bergeron et al., 2010). But the requirement of high torque due to the relatively high viscosity of hydrate solution added to appropriate sealing needed for shaft insertion assembly significantly increase the capital costs. Furthermore, the scale up of system with a stirrer is not economically reasonable since the power required for stirring generally increases with the 5^{th} power of the impeller size, which depends on the reactor size (Mori, 2003).

Other types of small scale reactors were also developed like the continuous flow reactor (Yang et al., 2008), the static mixer reactor (Tajima et al., 2004), and a reactor with porous silica gel adsorbent to increase contact area between gas and water phases (Seo et al., 2005).

The system proposed in this work is a high pressure slurry bubble column, operating in the semi-continuous mode, where the hydrate forming gas is introduced at the bottom of the

reactor which initially contains the water. The heat produced by the hydrate formation is continuously removed by the means of a cooling jacket so that temperature can be maintained.

1.4 Research objectives

An efficient method of converting gas into hydrate is considered in this work. The reactor chosen is a slurry bubble column and will be used to make carbon dioxide hydrates. This gas was selected for safety reasons because of its chemical inertness compare to other natural gas components such as methane. But the main motivation is to study hydrate production and observe phenomenon that would be similar with natural gas at other conditions. The specific objectives of the research are:

1- Understand the factors affecting heat transfer and bubble dynamic in a gas-liquid-solid system for which the solid phase is less dense than the liquid phase, as it would be the case in a system involving natural gas-water-hydrate. Since hydrate formation is an exothermic process, it is important to well understand the parameters that will influence the capacity of heat removal of the reactor.

2- Produce carbon dioxide hydrate in a slurry bubble column, study the rate of production of carbon dioxide hydrate and observe phenomena at different operating conditions in term of gas velocity, temperature and pressure.

It is to be noted that the two objectives were accomplished in parallel. During the preparation/adjustments of the high pressure slurry bubble column reactor, experiments on heat transfer in the atmospheric three-phase inverse fluidized bed were performed.

1.5 Research outline

In order to well understand the factors affecting the heat transfer and the bubble dynamic in a gas-liquid-solid system for which the solid phase is less dense than the liquid phase, it is necessary to perform experiments since no data is available at our operating conditions and column scale. The effect of natural gas hydrate was simulated using polypropylene particles which are less dense than water. Gas holdup, average heat transfer coefficient and other statistical features were assessed for different solid concentration, gas velocity, and liquid velocity with the presence or not of a surfactant to inhibit bubble coalescence (resulting in small bubbles and similar holdup to those in a high pressure system). This work is entitled as: “Heat transfer and bubble dynamics in a three-phase inverse fluidized bed” and presented in Chapter 2.

The formation of natural gas hydrate in a slurry bubble column is seen as a potential avenue for large scale production for transportation and storage. However, there is no data on hydrate production in a bubble column with a relatively large diameter at gas velocities involving significant phase mixing. Better mixing will enhance the interfacial area between the phases, resulting in a greater hydrate production rate. Thus, carbon dioxide hydrates were produced to simulate phenomena that would be observed during the formation of natural gas hydrate. The effects of operating conditions such as gas velocity, temperature and pressure

were assessed to gain insight on the role of these parameters on the hydrate production rate. This work is entitled as: "Synthesis of CO_2 hydrates in a slurry bubble column" and presented in Chapter 3.

Finally, Chapter 4 summarizes conclusions and recommendations for future research.

References

Aaron, D., Tsouris, C., (2005). Separation of CO2 from Flue Gas: A Review. Separation Science and Technology, 40(1), 321-348.

Bergeron, S., Beltran, J.G., Servio, P., (2010). Reaction rate constant of methane clathrate formation. Fuel 89, 294-301.

Council of Canadian Academies, The expert panel on gas hydrates, (2008). Energy from gas hydrates: Assessing the opportunities & challenges for Canada.

Fan, S., Li, S., Wang, J., Lang, X., Wang, Y., (2009). Efficient capture of CO_2 from simulated flue gas by formation of TBAB or TBAF semiclathrate hydrates. Energy fuels, 23(8), 4202-4208.

Fujita, S., Watanabe, K., Mori, Y.H, (2009). Clathrate-hydrate formation by water spraying onto porous metal plate exuding a hydrophobic liquid coolant. American institute of Chemical Engineering, 55(4), 1056-1064.

Giavarini, C., Miccioni, F., (2004). Self-perservation at low pressures of methane hydrates with various gas contents. Industrial and engineering chemistry research, 32, 1251-1274.

Gudmundsson, J.S., Borrehaug, A., (1996). Frozen hydrate for transport of natural gas. In: Proceeding of the 2th International Conference on Gas Hydrates, Toulouse.

Iwasaki, T., Katoh, Y., Nagamori, S., Takahashi, S., Oya, N., (2005). Continuous natural gas hydrate pellet production (NGHP) by process development unit (PDU). In: Proceeding of the 5th International Conference on Gas Hydrates, Trondheim.

Kanada, H., (2006). Economic study on natural gas transportation with natural gas hydrate (NGH) pellets. 23rd World Gas Conference, Amsterdam.

Kobayashi, T., Imura, N., Ohmura, R., Mori, Y.H., (2007). Clathrate hydrate formation by water spraying in a methane + ethane + Propane gas mixture : Search for the rate-controlling mechanism of hydrate formation in the presence of methylcyclohexane. Energy and Fuels, 21, 545-553.

Kang, S-P., Lee, H., (2000) Kang and Lee, (2000). Recovery of CO_2 from Flue Gas Using Gas Hydrate: Thermodynamic verification through phase equilibrium measurements. Environmental science and technology, 34, 4397-4400.

Koh, C.A., Sloan, D.S., (2007). Natural gas hydrates: Recent advances and challenges in energy and environmental applications. American Institute of Chemical Engineering, 53(7), 1636-1643.

Lee, J.D, Susilo, R., Englezos, P., (2005). Kinetics of structure H gas hydrate. Energy and fuels, 19, 1008-1015.

Lee, S., Liang, L., Riestenberg, D., West, O.R., Tsouris, C., Adams, E., (2003). CO_2 hydrate composite for ocean carbon sequestration. Environmental science and technology, 37, 3701-3708.

Li, S.F., Fan, S.S., Wang, J.Q., Lang, X.M., Liang, D.Q., (2009). CO_2 capture from binary mixture via forming hydrate with the help of tetra-n-butyl ammonium bromide. Journal of natural gas chemistry, 18(1), 15-20.

Linga, P., Kumar, R., Lee, J.D., Ripmeester, J., Englezos, P., (2010). A new apparatus to enhance the rate of gas hydrate formation: Application to capture of carbon dioxide. International Journal of Greenhouse Gas Control, 4, 630-637.

Luo, Y.T., Zhu, J.H., Fan, S.S., Chen, G.H., (2007). Study on the kinetics of hydrate formation in a bubble column. Chemical engineering science, 62, 1000-1009.

Matsuda, S., Tsuda, H., Mori, Y.H., (2006). Hydrate formation using water spraying onto a cooled solid surface in a guest gas. American institute of chemical engineering, 52(8), 2978-2987.

Mori, Y.H., (2003). Recent advances in hydrate-based technologies for natural gas storage- a review. Journal of chemical industry and engineering. CAS Symposium of gas hydrate, 54.

Mork, M., Gudmundsson, J.S., (2002). Hydrate formation rate in a continuous stirred tank reactor: Experimental results and bubble-to-crystal model. In: Proceeding of the 4th International Conference on Gas Hydrates, Yokohama.

Murakami, T., Kuritsuka, H., Fujii, H., Mori, Y.H., (2009). Forming a structure-H hydrate using water and methlycyclohexane jets impringing on each other in a methane atmosphere. Energy and Fuels, 23, 1619-1625.

Seo, Y-T., Moudrakovski, I., Ripmeester, J.A., Lee, J-W., Lee, H., (2005). Efficient recovery of CO2 from flue gas by clathrate hydrate formation in porous silica gels. Environmental Science and Technology, 39, 2315-2319.

Sloan, E.D., Koh, C.A., (2008). Clathrate Hydrates of natural gases. 3rd ed., Boca Raton, FL., CRC Press.

Tajima, H., Yamasaki, A., Kiyono, F., (2004). Continuous formation of CO_2 hydrate via a kenics-type static mixer. Energy and fuels, 18, 1451-1456.

Thomas, S., Dawe, R.A., (2003). Review of ways to transport natural gas energy from countries which do not need the gas for domestic use. Energy, 28, 1461-1477.

Watanabe, S., Takahashi, S. Mizubayashi, H., Muratal, S., Murakami, H., (2008). A demonstration project of NGH lad transportation system. In: Proceeding of the 6th International Conference on Gas Hydrates, Vancouver.

Yang, D., Le, A., Martinez, R.J., Currier, R.P. Spencer, D.F., Deppe, G., (2008). Heat transfer during CO_2 hydrate formation in a continuous flow reactor. Energy and fuels, 22, 2649-2659.

Web sites:

US Environmental Protection Agency, http://www.epa.gov/methane/, consulted on November 10th, 2010

Mitsui Engineering & Shipbuilding Co., Natural Gas Hydrate Project, http://www.mes.co.jp/english/business/energy/energy_09.html, consulted on November 10th, 2010.

Chapter 2 - Heat transfer and bubble dynamics in a three-phase inverse fluidized bed

Denis Myre and Arturo Macchi*

Department of Chemical and Biological Engineering, University of Ottawa,

161 Louis Pasteur, Ottawa, Ontario, Canada K1N 6N5

Chemical Engineering and Processing: Process intensification, (2010), 49(5), 523-529

Abstract

In this study, surface-to-bed heat transfer experiments were performed to gain insight on heat transfer and hydrodynamics in a three-phase inverse fluidized bed. Air, tap water or 0.5% wt. aqueous ethanol, and polypropylene were respectively the gas, liquid and solid phases. The solid loading was varied from 0 to 30% vol., and the gas and liquid superficial velocities from 2 to 50 mm/s and 0 to 21 mm/s, respectively. Visual observations were associated with measured phase holdups and instantaneous heat transfer coefficients. Larger gas velocities lead to an increase in bubble size due to the transition to the coalesced bubble flow regime. The greater turbulence induced by the larger bubbles increases the average heat transfer coefficient. On the other hand, adding ethanol reduces the heat transfer coefficient. Solid concentrations up to ~13% vol. increase the average heat transfer coefficient whereas higher solid concentrations tend to lower it. The distribution of instantaneous heat transfer coefficient peak height is wider at higher gas and liquid velocities while the addition of a surfactant narrows it. Gas holdups and average heat transfer coefficients are both compared with existing correlations, which are then adjusted for a better fit.

2.1 Introduction

Three-phase inverse fluidized beds involve solid particles with a density lower than the liquid phase. The rise of gas bubbles causes the particles to fluidize downwards, while the liquid flowing counter-current to the gas intensifies this behaviour. These systems are recognized for their relatively high rates of mass and heat transfer. They are especially employed in processes that exploit bacteria such as food fermentation and wastewater treatment as a way of controlling the biofilm thickness on the support particles [1,2].

Compared to conventional fluidized beds, fewer studies have been performed on three-phase inverse fluidized beds. Moreover, most experiments have focused on hydrodynamics [3-13] and mass transfer [10,14-17]. Heat transfer was less investigated [10,18,19], with experiments limited to superficial gas velocities below 8 mm/s. Temperature control of reactors is key for maintaining optimal rates of reaction, but also for indirectly regulating the rates of mass transfer since fluid properties (viscosity, density and diffusivity) are function of temperature. Moreover, when microorganisms are involved, their environment must be closely controlled to insure their proliferation and proper activities. Hence, for industrial applications, the understanding of heat transfer phenomena over a larger range of flow conditions is necessary.

In this present work, we thus evaluate the average surface-to-bed heat transfer coefficient in a three-phase inverse fluidized bed for a greater range of superficial gas velocities and bed expansions. Furthermore, analysis of the instantaneous heat transfer coefficient is performed to provide more information on hydrodynamics [20-22], particularly on bubble dynamics.

Finally, we examine the effect of the presence of a surfactant, as it would be found in biological reactors.

2.2 Experimental

The three phases of the system are air, tap water or 0.5%wt. aqueous ethanol solution and polypropylene particles (d_p = 2.7 mm, ρ_S = 880 kg/m^3, ϕ = 0.86). For the liquid-solid system, the particle Richardson-Zaki index and terminal velocity were experimentally estimated at 2.69 and 74 mm/s, respectively. The minimum fluidization for the same system was measured at 5.1 mm/s. The system was run under ambient temperature and pressure both in the liquid batch mode (i.e. inverse turbulent bed, [9]) and with counter-current gas and liquid flow.

The experimental column is constructed of acrylic with an effective length of 2.15 m, and an inner diameter of 0.152 m, sufficiently large to minimize wall effects on overall phase holdups [23]. The liquid phase is introduced at the top of the column. The liquid volumetric flow rate is adjusted to reach a constant hydrostatic head and steady-state operation. The gas is introduced at the bottom of the column via two perforated tubes arranged in a cross section with a total of 16 holes having a diameter of 0.838 mm. Rotameters monitor the liquid and gas flow rates. A schematic of the experimental system can be found elsewhere [17]. All data were evaluated for superficial gas and liquid velocities of U_g = 2-50 mm/s and U_L = 0-21 mm/s, respectively, as well as for solids loadings of M = 0-9.2 kg representing solid volumetric concentrations between 0% and 30%. Under these conditions, the bed can expand to different levels until it reaches the gas distributor. A good description of the different levels of expansion in an inverse turbulent bed is given by Comte et al. [4]. In our study, the

bed did not expanded beyond the gas distributor where there are no longer any rising gas bubbles creating liquid backmixing and hence the buoyant force on the particles acts to draw them back up into the bed.

Overall phase holdups were obtained by measuring the dynamic pressure drop along the column at several levels. A differential pressure transducer, model PX750-30DI from Omega, was used with a reference pressure tap situated 57 mm below the top liquid distributor. The bed height, H_b, and resulting solid holdup, ε_S, are determined from the intersection of the bed and freeboard pressure drop lines, each obtained by linear regression.

$$\varepsilon_S = \frac{4M}{\pi D^2 H_b \rho_S} \qquad (2.1)$$

Neglecting the frictional drag on the wall and accelerations of the phases in the vertical direction, the gas holdup, ε_G, is related to the dynamic pressure drop, $-\Delta P$, by

$$\varepsilon_G = \left(\varepsilon_S\left(\rho_S - \rho_L\right) + \Delta P / g\Delta z\right)/\left(\rho_L - \rho_G\right) \qquad (2.2)$$

Finally, the liquid holdup, ε_L, is obtained by

$$\varepsilon_L = 1 - \varepsilon_G - \varepsilon_S \qquad (2.3)$$

The heat transfer probe is constructed from a 63.5 mm long brass cylinder. The inner and outer diameters are respectively 6.35 mm and 12.7 mm. The cylinder is capped at both ends with threaded Teflon to ensure a watertight fit and no axial heat loss. At one end, the Teflon serves as connector to attach the probe to a stainless steel support tube. A cartridge heater (Thermal Corporation, Model CL) is inserted in the probe cavity. Its length is 50.8 mm, its diameter is 6.35 mm and it generates 168 W at 60 V. Two fast response type-T thermocouples (Omega, Model C-01-T) were fixed on the surface of the probe at two

different locations in order to measure instantaneous surface temperature. By measuring the bulk temperature of the bed with an additional Type-T thermocouple, the instantaneous heat transfer coefficient is calculated as follow:

$$h_i = \frac{Q_i}{A(T_{S,i} - T_{bulk,i})} \qquad (2.4)$$

The average coefficient of variation for the gas holdup (1%) and average heat transfer coefficient (2%) were calculated from three samples of data acquisition for each operating gas velocity in the bubble column.

The standard deviation and skewness of the instantaneous heat transfer coefficient distribution can be used as indicators for bubble size distribution [22]. The skewness is a measure of the asymmetry of the probability distribution of a real-valued random variable. If the data are symmetrically distributed around the mean, the skewness is equal to zero. It is positively skewed when the extreme values are concentrated on the right of the curve, and negatively skewed when the extreme values are concentrated at the left of the curve. The skewness is calculated as follow:

$$\gamma = \frac{N}{(N-1)(N-2)} \sum \left(\frac{h_i - h_{average}}{h_{stdev}} \right)^3 \qquad (2.5)$$

The peak height distribution of the instantaneous heat transfer coefficient may give a good insight on hydrodynamics, particularly to understand the role of bubbles on heat transfer at different operating conditions. Li and Prakash [21] found that the peak height was not uniformly distributed for a given operating condition. As a result, they developed a peak-height fitting method to obtain the distribution of peak heights. They divided the peak heights into equally spaced intervals of 500 W/m^2°C and chose a baseline that is equal to the

average of heat transfer coefficient values that are lower than the overall average. The peak height was defined as a local maximum heat transfer coefficient for a passing bubble-wake between two local minima, minus the baseline value [21]. This methodology is used in this study to link the instantaneous heat transfer signal to the bubble dynamics in a three-phase inverse fluidized bed.

2.3 Results and discussion

Presentation and interpretation of experimental data will be first performed for a bubble column and then a three-phase inverse fluidized bed. Correlation of data is also carried out.

2.3.1 Bubble column

Figure 2.1 shows the gas holdup as a function of gas velocity for two different downward liquid velocities. The gas holdup increases with increasing gas velocity. For tap water, the transition from a dispersed to coalesced bubble flow regime corresponds approximately to the decrease in the slope of ε_G vs. U_g, whereas no such drop is observed in the presence of ethanol. Although higher gas velocities produce a larger distribution of bubble sizes, the presence of microbubbles in the aqueous ethanol solution has an important effect on the overall gas holdup. Froth became apparent near the flow regime transition point due to the combined effect of the surfactant and intense mixing induced by the larger and faster rising bubbles along the column centerline. The jetting of gas at the distributor can also contribute to the formation of microbubbles at high gas velocity. Figure 2.1 also shows that an increase in liquid velocity results in a greater gas holdup. Water flowing downwards increases the drag and reduces the bubble rise velocity, thus increasing the bubble residence time.

Visually, the bubble rise was hindered, particularly close to the wall, when the liquid velocity increased.

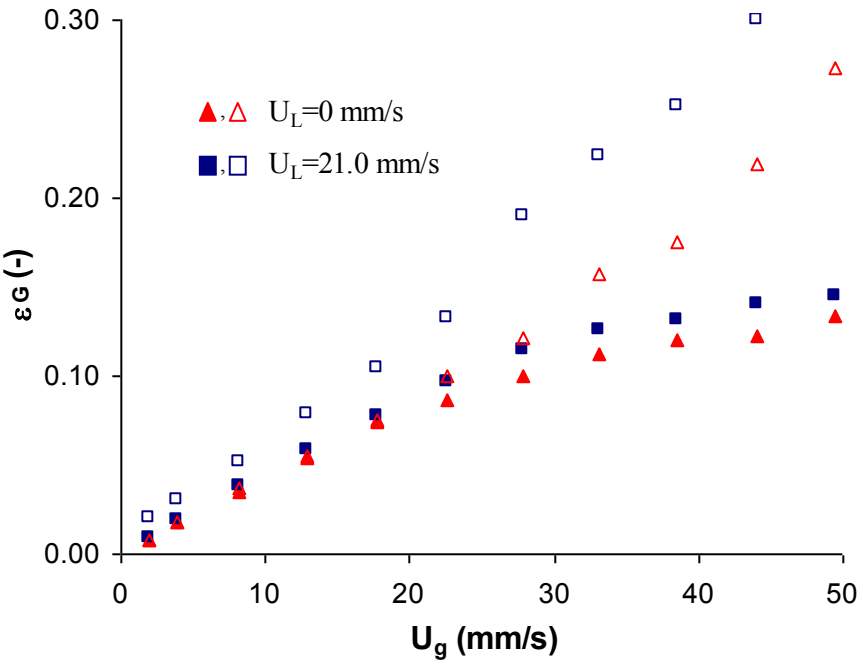

Figure 2.1: Gas holdup as a function of superficial gas velocity for different superficial liquid velocities in a bubble column for tap water and 0.5% wt. aqueous ethanol solution. Open symbols represent aqueous ethanol data.

The time-average heat transfer coefficients for the same conditions are depicted in Figure 2.2. It can be seen that $h_{average}$ increases with rising gas velocity. The rate of surface renewal engendered by the passage of bubbles increases with bubble frequency and size. The presence of ethanol has a small effect in lowering the average heat transfer coefficient. Since the probe was located at the centerline of the column, the turbulence created by the passage of larger and faster rising bubbles at the higher gas velocities was similar for both systems. The average heat transfer coefficient is thus mainly controlled by the larger bubbles rather than the microbubbles. For a given liquid solution, the value of $h_{average}$ is less sensitive to the liquid velocity because it does not significantly influence the flow regime.

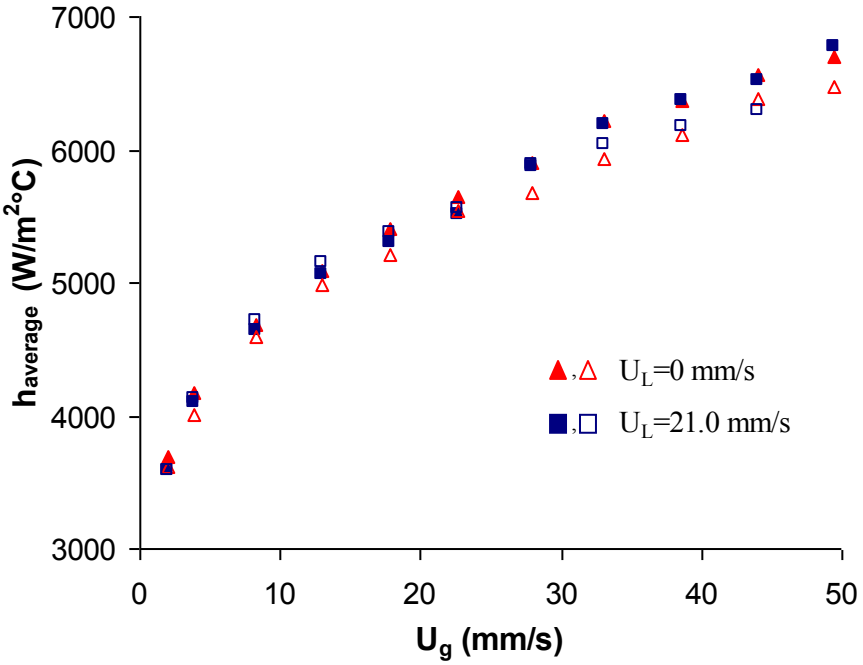

Figure 2.2: Average heat transfer coefficient as a function of superficial gas velocity for different superficial liquid velocities in a bubble column for tap water and 0.5% wt. aqueous ethanol solution. Open symbols represent aqueous ethanol data.

Figures 2.3 and 2.4 present the statistics on the heat transfer coefficient distribution. The h_{stdev} and skewness increase with rising gas velocity due to a greater bubble size distribution. Moreover, the heat transfer coefficient distribution is positively skewed meaning that extreme values are higher than typical values. However, these metrics were not sufficiently sensitive to measure a considerable effect of liquid velocity or surfactant, again probably due the similar bubble dynamics at the centerline.

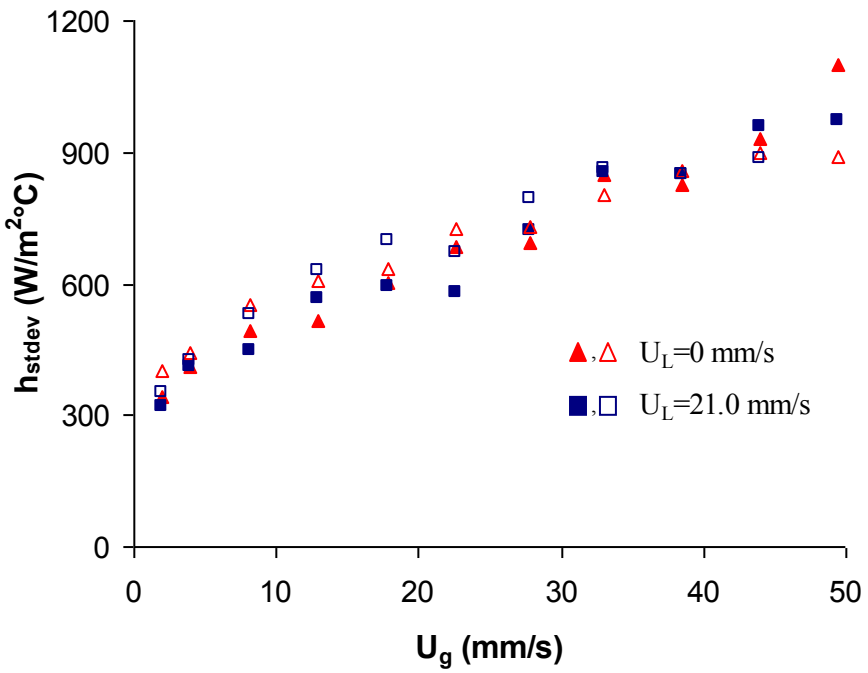

Figure 2.3: Standard deviation of instantaneous heat transfer coefficient as a function of superficial gas velocity for different superficial liquid velocities in a bubble column for tap water and 0.5% wt. aqueous ethanol solution. Open symbols represent aqueous ethanol data.

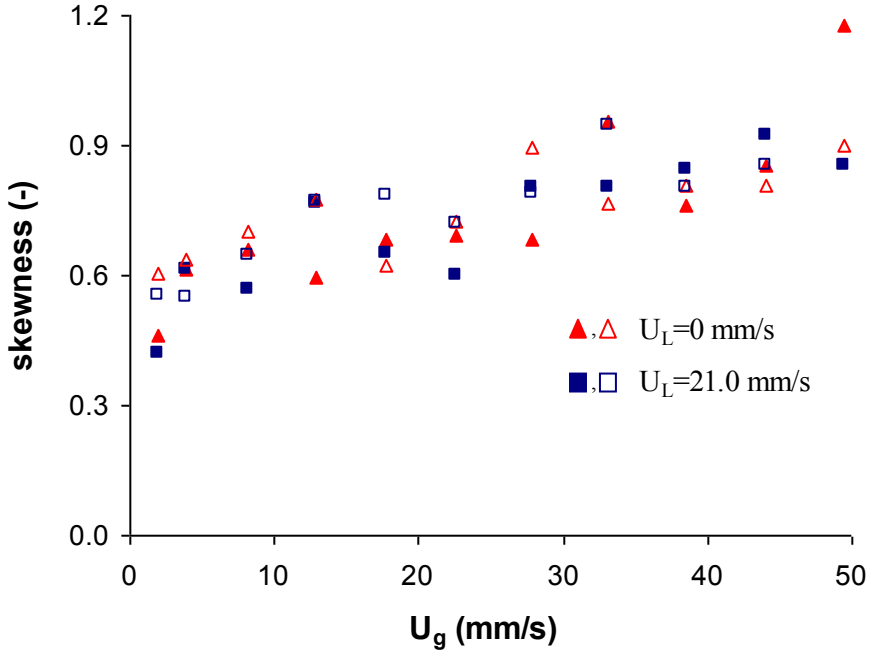

Figure 2.4: Skewness of instantaneous heat transfer coefficient as a function of superficial gas velocity for different superficial liquid velocities in a bubble column for tap water and 0.5% wt. aqueous ethanol solution. Open symbols represent aqueous ethanol data.

2.3.2 Three-phase inverse fluidized bed

2.3.2.1 Effect of gas velocity and solid loading

The quantities of polypropylene particles were chosen in order to obtain solid concentrations from 0 to 30% vol. at full expansion of the bed. Figure 2.5 illustrates the phase holdups as a function of superficial gas velocities for different solid loadings (M) in tap water at $U_L = 0$. Full expansion of the bed is attained at relatively low superficial gas velocities (between 17.5 and 23.0 mm/s) and higher solid loading reduces the gas velocity required to attain this point. The gas holdup increases with increasing gas velocity and decreasing solids loading. The effect of particles is primarily seen in the coalesced bubble flow regime, which is induced earlier as the particles promoted bubble coalescence. Finally the liquid holdup (ε_L) increases at low gas velocity and then decreases once the full bed expansion is achieved.

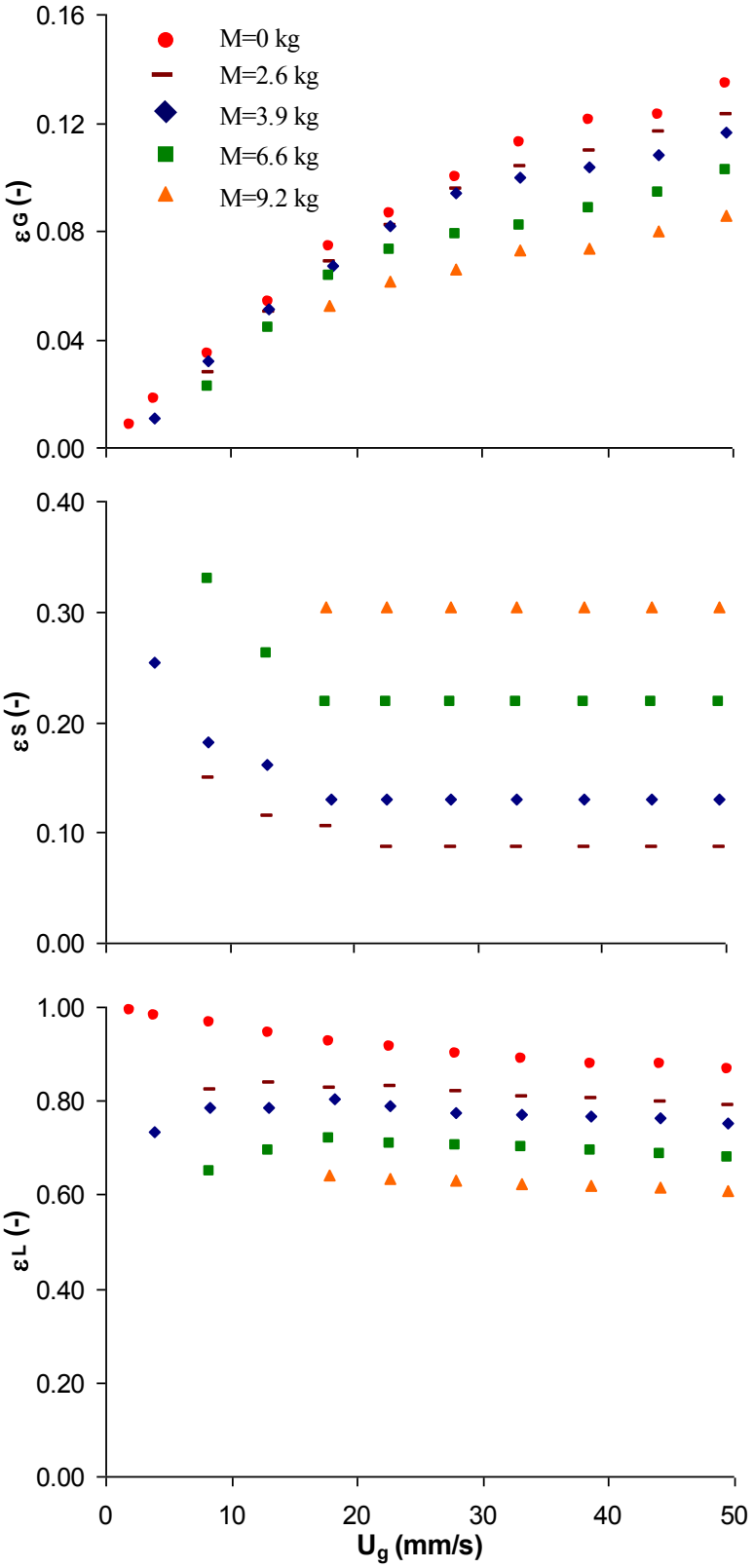

Figure 2.5: Phase holdups as a function of superficial gas velocity at U_L= 0 and different solid loading for tap water.

Figure 2.6 shows the influence of gas velocity and solid holdup on the time-averaged heat transfer coefficient. As observed by others, the heat transfer coefficient increases with increasing gas velocity [10,18,19]. Since larger bubbles have greater rise velocities and larger wakes, the bubble-induced turbulence increases with gas velocity. The distribution of the instantaneous heat transfer coefficient peak height in Figure 2.7 also shows the effect of gas velocity on bubble dynamics. At low gas velocity, the distribution of peak height is small since the flow regime is dispersed and the bubble size distribution is more uniform. At higher gas flow rates, the distribution is wider because of the larger distribution of bubble size in the coalesced bubble flow regime. Furthermore, the distribution is displaced to the right when gas velocity increases meaning that the average bubble size increases.

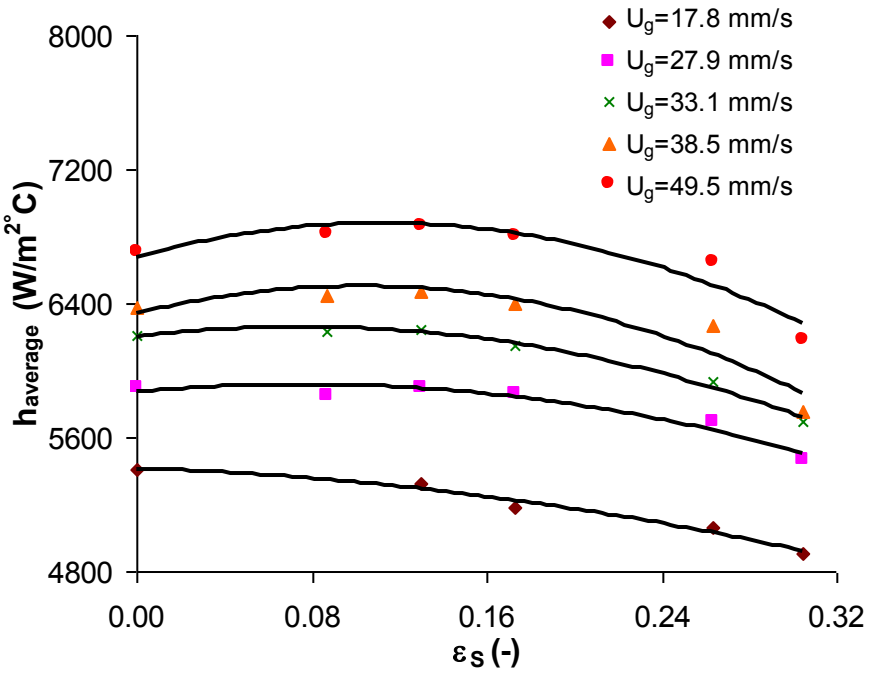

Figure 2.6: Average heat transfer coefficient as a function of solid holdup at different gas velocities for tap water and U_L = 0.

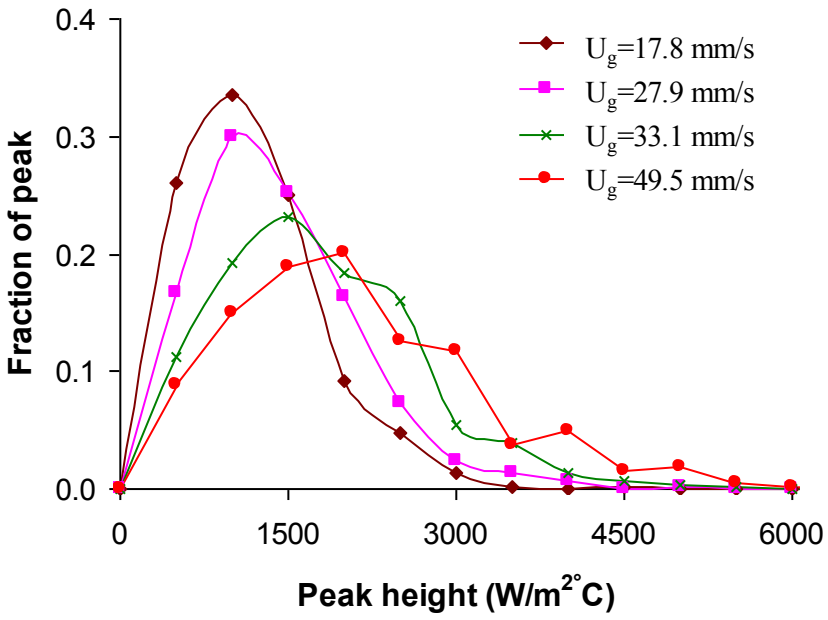

Figure 2.7: Instantaneous heat transfer coefficient peak height distribution at different superficial gas velocities for tap water at U_L = 0 and M = 3.9kg.

From Figure 2.6, an increase in the average heat transfer coefficient is observed up to a concentration of around 13% vol. solid. This trend is associated with the contact frequency between the particles and the surface of the probe which enhances the surface renewal of the fluid at the vicinity of the probe. Above a concentration of 13%, the average heat transfer coefficient decreases due to an increase in the liquid-solid slurry apparent viscosity. The same phenomenon was observed in a classical three-phase fluidized bed [24]. In an air-water-glass beads (d_p =35μm) slurry bubble column, Li and Prakash observed a continuous decrease of the heat transfer coefficient for solids loading up to 40% vol [25].

As in the gas-liquid system, the standard deviation and skewness of the instantaneous heat transfer coefficient distribution increased with rising gas velocity, but was again not sufficiently sensitive to identify the effects of particles on bubble dynamics.

2.3.2.2. Effect of liquid velocity and surfactant

The following figures present the effect of liquid velocity and surfactant with a particle loading of 3.9 kg. From Figure 2.8, the gas velocity at which the bed is fully expanded decreases when increasing the liquid velocity or adding ethanol. For the tap water system, gas holdups are not significantly affected by U_L up to 21 mm/s. Cho et al. obtained similar results within the same range of liquid velocities [18]. Competing effects may be occurring. The downward flow of liquid increases the bubbles residence time in the column, thus increasing the gas holdup. As the liquid velocity increases, it was visually observed that the bubble rise was impeded, particularly close to the wall. On the other hand, the liquid flowing downward promotes coalescence of small bubbles, lowering the gas velocity required to reach the coalesced bubble flow regime. It is consistent with visual observations since the flow regime entered coalesced bubble flow at U_g around 33, 23 and 18 mm/s when the liquid velocities were 0, 8.8 and 21.0 mm/s, respectively. Since larger bubbles have a greater rise velocity, it decreases the gas holdup. Thus for the liquid velocities studied, the phase holdups were similar but a difference exists in the distribution of bubble sizes as shown by the distribution of instantaneous heat transfer coefficient peak heights in Figure 2.12.

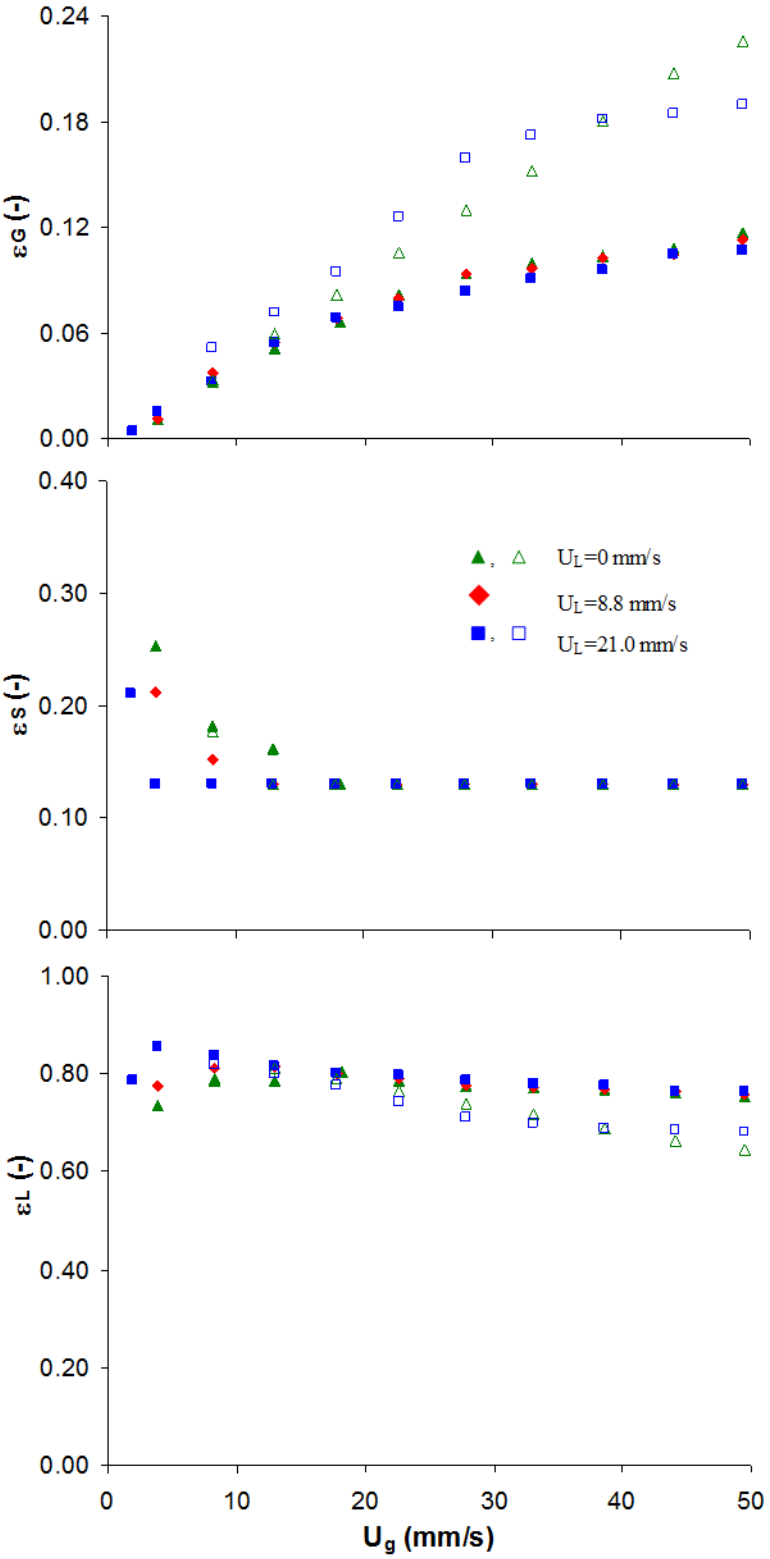

Figure 2.8: Phase holdups as a function of superficial gas velocity at different superficial liquid velocities for M = 3.9 kg. Open symbols represent aqueous ethanol data.

Surfactants increase gas holdups and influence the transition point between the dispersed and coalesced bubble flow regimes by creating surface tension gradients that immobilize the interface and prevent bubble coalescence resulting in smaller bubbles with lower rise velocities and longer residence times. For gas velocities below 15 mm/s, the presence of ethanol does not greatly affect bubble dynamics since the regime is in dispersed bubble flow for both liquids and bubble diameters are similar (< 10 mm). At higher gas velocity, the effect of ethanol is more obvious. When $U_L = 0$, the tap water system enters the coalesced bubble flow regime whereas visually the flow regime for the aqueous ethanol solution was in transition at the higher gas velocities. The aqueous ethanol solution still formed a froth of microbubbles due to the presence of some larger bubbles and the start of more intense liquid mixing. As a result, no decrease in the slope of ε_G vs. U_g is observed. Similar findings were reported for the gas-liquid system in Figure 2.1. However, at $U_L = 21$ mm/s, a change in the flow regime was observed for both tap water at $U_g \approx 18$ mm/s and aqueous ethanol at $U_g \approx 30$ mm/s. The impact of downward flowing liquid on bubble dynamics is thus more significant with ethanol present as gas holdups are greater in dispersed bubble flow and lower if the coalesced bubble flow regime is induced.

The effect of liquid velocity and surfactant on the average heat transfer coefficient is illustrated in Figure 2.9. As with the overall gas holdup, their impact is consistent with the flow regime and resulting bubble size distribution, which affects the fluid renewal at the surface of the probe. Moreover, the rate of increase in $h_{average}$ with U_g is lower in coalesced bubble flow than in dispersed bubble flow. The bubble-induced turbulence may increase with gas velocity, but more of the probe is covered by the gas phase.

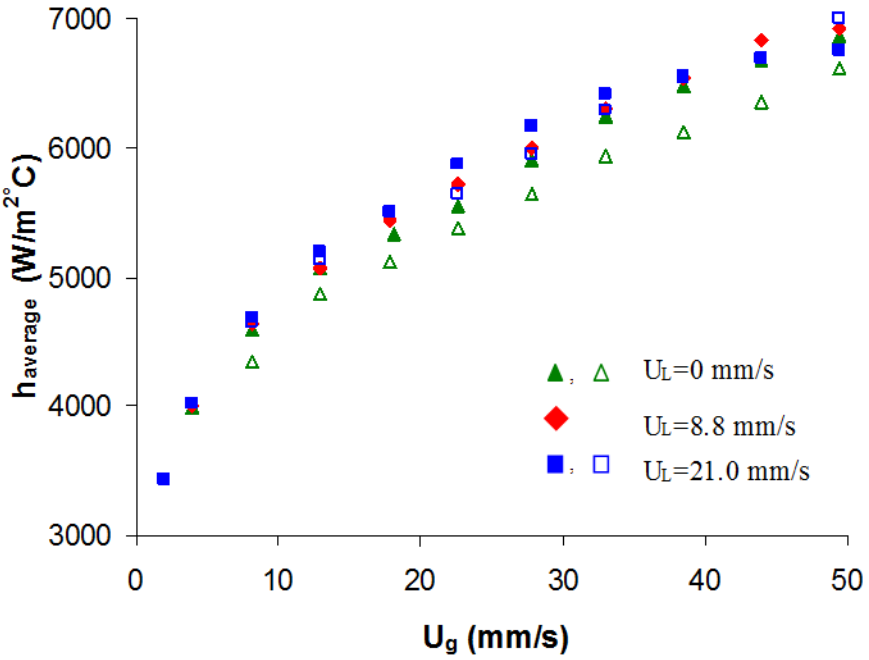

Figure 2.9: Average heat transfer coefficient as a function of superficial gas velocity at different superficial liquid velocities for M=3.9 kg. Open symbols represent aqueous ethanol data.

Figures 2.10 to 2.12 corroborate with previously discussed aspects concerning the effect of ethanol and liquid velocity on bubble dynamics at the column centerline. From Figure 2.10, the standard deviation of instantaneous heat transfer coefficient in the ethanol solution increases with increasing gas and liquid velocities due to bubble coalescence and a greater bubble size distribution. Figure 2.11 presents the distribution of instantaneous heat transfer coefficient peak heights for the two liquid solutions. The aqueous ethanol solution shows a similar distribution to tap water, but is slightly displaced to lower values.

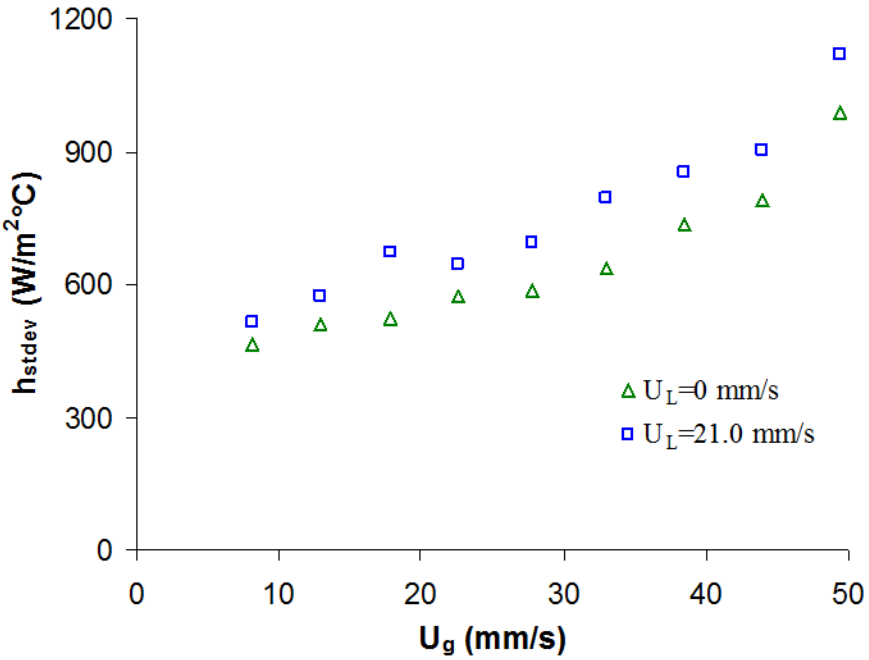

Figure 2.10: Standard deviation of instantaneous heat transfer coefficient as a function of superficial gas velocity at different superficial liquid velocities for 0.5% wt. aqueous ethanol solution (M = 3.9kg).

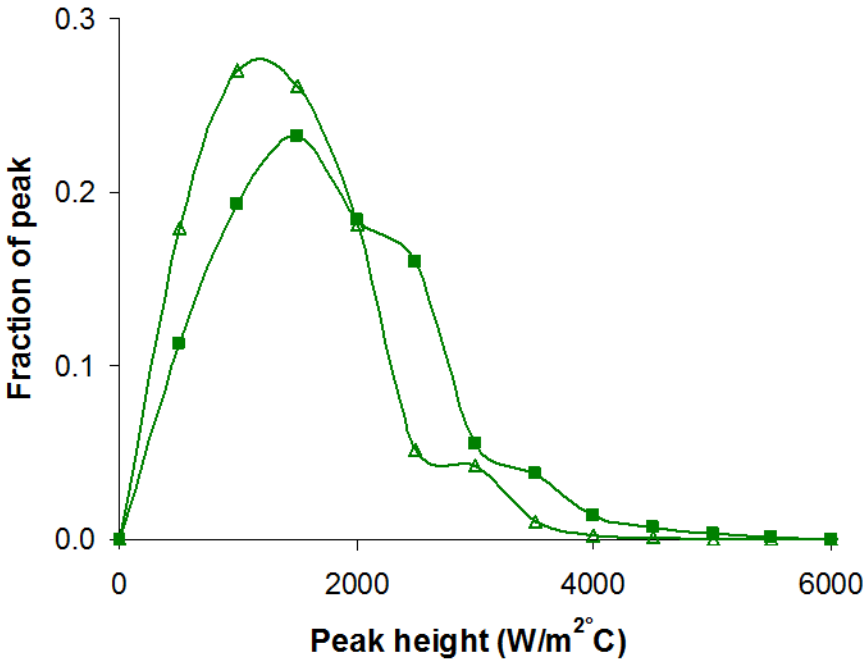

Figure 2.11: Instantaneous heat transfer coefficient peak height distribution for tap water and 0.5% aqueous ethanol at U_g = 33.1mm/s, U_L = 0 and M = 3.9kg. Open symbols represent aqueous ethanol data.

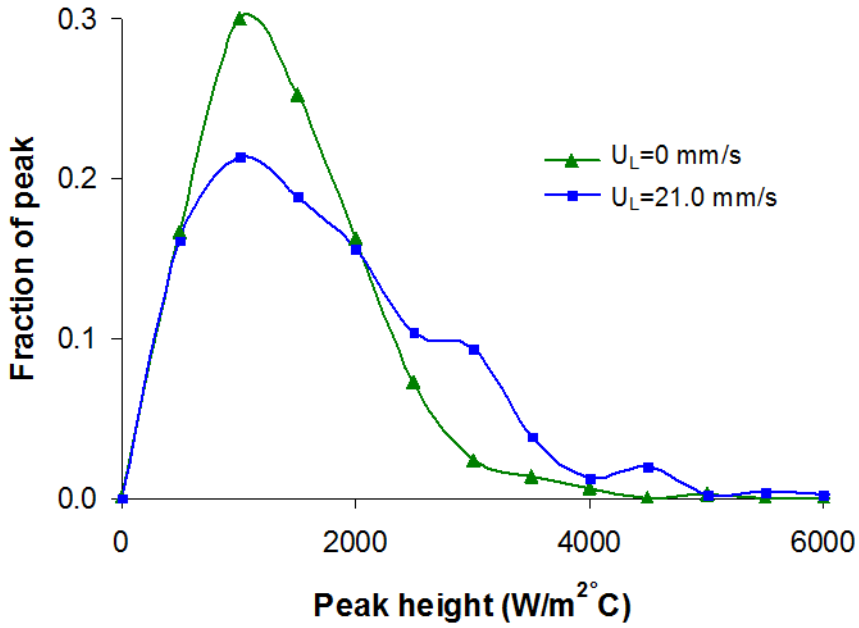

Figure 2.12: Instantaneous heat transfer coefficient peak height distribution at different superficial liquid velocities for tap water (U_g = 27.9 mm/s) and M = 3.9 kg.

2.3.3 Correlations for phase holdups and heat transfer coefficient

The gas holdups were correlated with the equation of Behkish et al. for slurry bubble columns [26]. With their original correlation, an average absolute relative error (AARE) of 42% and a bias factor (F_m) of 0.58 were found. This discrepancy is likely due to the geometrical effect of the gas distributor on the bubble formation. As the correlation consistently underestimated the experimental data, the AARE was minimized to 9% by adjusting the leading constant parameter to 0.00874 instead of the original value of 0.00494.

The experimental Nusselt numbers were compared to those predicted by the correlation proposed by Son et al. for three-phase inverse fluidized beds [19]:

$$h = C\left[k_L \rho_L C_{PL} \left\{\left[\left(U_L + U_g\right)\left(\rho_L \varepsilon_L + \rho_G \varepsilon_G + \rho_S \varepsilon_S\right) - \left(U_g \rho_G\right)\right] g / \varepsilon_L \mu_L\right\}^{1/2}\right]^{1/2} \qquad (2.6)$$

$$Nu = \frac{h d_p \left(1 - \varepsilon_S\right)}{k_L \varepsilon_S} \qquad (2.7)$$

Data acquired from the experiments with the ethanol solution were included since bubble dynamics were found to be similar at the centerline of the column for both systems. An AARE of 59% and a bias F_m of 0.41 were found. The discrepancy may be due to the relatively large length of the heat transfer probe used by Son et al. [19] since this can potentially affect fluid properties in the vicinity of the probe. The temperature gradient between the bulk and probe surface could have decreased along the length of the probe resulting in lower heat transfer coefficients. As a result, the AARE was minimized to 6% by modifying the leading constant parameter to 0.145 instead of 0.058. Figure 2.13 shows the similitude between the experimental and the predicted values from the modified equation.

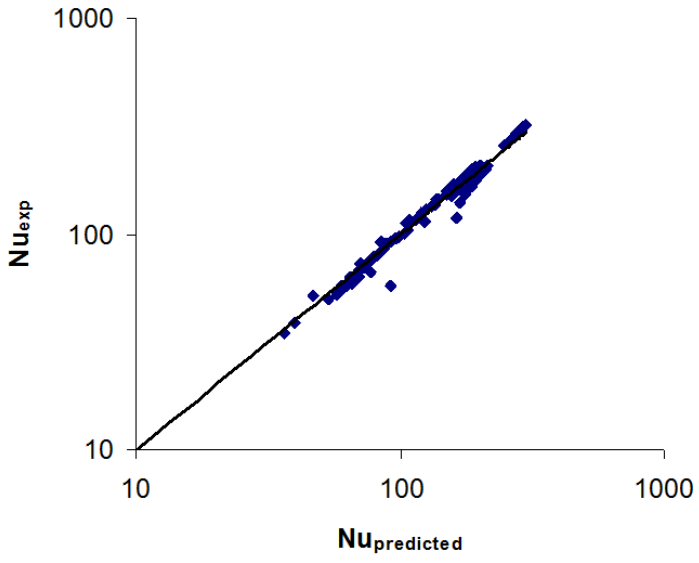

Figure 2.13: Experimental Nusselt number vs. predicted Nusselt number (modified correlation of Son et al. [19].

2.4 Conclusion

The effects of gas and liquid superficial velocities, solids loading and the presence of a surfactant on heat transfer and hydrodynamics were studied in a three-phase inverse fluidized bed. The average heat transfer coefficient measured at the column centerline increased with superficial gas velocity and liquid velocity since bubble coalescence is promoted. The addition of ethanol as a surfactant mainly affected gas holdups at the higher gas velocities where mixing is intense and a froth of micro-bubbles is formed. The surfactant also slightly reduced the heat transfer coefficient by decreasing the amount and size of larger bubbles. Solid holdups below ~13% increase the average heat transfer coefficient while greater solid holdups lower it. The increase in the standard deviation and a positive skewness of the instantaneous heat transfer coefficient signal as well as the distribution of peak height all supported visual observations of larger bubble size distributions at higher gas or liquid velocities. Gas holdups and average heat transfer coefficients were correlated with the equations of Behkish et al. [26] and Son et al. [19], respectively. The AAREs were minimized by changing the leading constant parameter in each equation.

Notation

A	cross sectional area of the heat transfer probe, m
AARE	average absolute relative error= $\frac{1}{j}\sum_{i=1}^{j} abs\left[\left(predicted - observed\right)/observed\right]$
C	leading constant parameter, equation of Son et al. [19]
C_{PL}	heat capacity of liquid phase, J/kg K
D	diameter of column, m
ΔP	dynamic pressure drop, Pa
d_p	diameter of sphere having same volume as particle, mm
F_m	Bias factor=$\exp\left[\frac{1}{j}\sum_{i=1}^{j}\ln\left(predicted/observed\right)\right]$

g	acceleration due to gravity, m/s^2
$h_{average}$	time-average heat transfer coefficient, $W/m^2°C$
H_b	bed height, m
h	heat transfer coefficient, $W/m^2°C$
h_i	instantaneous heat transfer coefficient, $W/m^2°C$
h_{stdev}	standard deviation of heat transfer coefficient, $W/m^2°C$
k_L	thermal conductivity of liquid phase, W/m°C
M	mass of particles, kg
N	number of data points
Nu	Nusselt number
Q_i	instantaneous heat transfer rate, W
$T_{bulk,\,i}$	temperature of the bulk at time i, °C
$T_{s,i}$	surface temperature of the probe at time i, °C
U_g	superficial gas velocity, m/s
U_L	liquid superficial velocity, m/s
Δz	axial distance between pressure measurement, m

Greek letters

$\varepsilon_G, \varepsilon_L, \varepsilon_S$	gas, liquid and solid holdup, dimensionless
μ_L	liquid viscosity, Pa.s
ρ_G, ρ_L, ρ_S	gas, liquid and particle density, kg/m^3
γ	skewness, dimensionless
ϕ	sphericity, dimensionless

Acknowledgment

The authors are grateful to the *Natural Sciences and Engineering Research Council of Canada* and to *Le Fonds Québécois de la Recherche sur la Nature et les Technologies* for financial assistance

References

[1] L. Nikolov, D. Karamanev, Experimental study of the inverse fluidized bed biofilm reactor, Can. J. Chem. Eng., 65 (1987) 214-217.

[2] M. Rajasimman, C. Karthikeyan, Aerobic digestion of starch wastewater in a fluidized bed bioreactor with low density biomass support, J. Hazard. Mater., 143 (2007) 82-86.

[3] Y.A.A. Ibrahim, C.L. Briens, A. Margaritis, M.A. Bergongnou, Hydrodynamic Characteristics of a Three-Phase Inverse Fluidized-Bed Column, AIChE J., 42 (1996) 1889-1900.

[4] M.P. Comte, D. Bastoul, G. Hebrard, M. Roustan, V. Lazarova, Hydrodynamics of a three-phase fluidized bed - The inverse turbulent bed, Chem. Eng. Sci., 52 (1997) 3971-3977.

[5] P. Buffière, R. Moletta, Some hydrodynamic characteristics of inverse three phase fluidized-bed reactors, Chem. Eng. Sci., 54 (1999) 1233-1242.

[6] D.H. Lee, N. Epstein, J.R. Grace, Hydrodynamic Transition from Fixed to Fully Fluidized Beds for Three-Phase Inverse Fluidization, Korean J. Chem. Eng., 17 (2000) 684-690.

[7] H.D. Han, W. Lee, Y.K. Kim, J.L. Kwon, H.S. Choi, Y. Kang, S.D. Kim, Phase hold-up and critical fluidization velocity in a three-phase inverse fluidized bed, Korean J. Chem. Eng., 20 (2003) 163-168.

[8] T. Renganathan, K. Krishnaiah, Prediction of minimum fluidization velocity in two and three phase inverse fluidized beds, Can. J. Chem. Eng., 81 (2003) 853-860.

[9] O. Sánchez, S. Michaud, R. Escudié, J.P. Delgenès, N. Bernet, Liquid mixing and gas-liquid mass transfer in a three-phase inverse turbulent bed reactor, Chem. Eng. J., 114 (2005) 1-7.

[10] D.K. Sang, Y. Kang, Hydrodynamics, heat and mass transfer in inverse and circulating three-phase fluidized-bed reactors for wastewater treatment, Stud. Surf. Sci. Catal., 159 (2006) 103-108.

[11] K. Il Lee, S. Mo Son, U. Yeong Kim, Y. Kang, S. Hwan Kang, S. Done Kim, J. Keun Lee, Y. Chil Seo, W. Hyun Kim, Particle dispersion in viscous three-phase inverse fluidized beds, Chem. Eng. Sci., 62 (2007) 7060-7067.

[12] I.S. Shin, S.M. Son, Y. Kang, Q.H. Kang, S.D. Kim, Phase holdup characteristics of viscous three-phase inverse fluidized beds, J. Ind. Eng. Chem., 13 (2007) 971-978.

[13] S.M. Son, S. H. Kang, U.Y. Kim, Y. Kang, S.D. Kim, Bubble properties in three-phase inverse fluidized beds with viscous liquid medium, Chem. Eng. Proc., 46 (2007) 736-741.

[14] V.R. Nikolov, I. Nikov, Liquid-solid mass transfer in three-phase inverse fluidized bed (TPIFB), Hung. J. Ind. Chem., 22 (1994) 125-128.

[15] V.R. Nikolov, I. Farag, I. Nikov, Gas-liquid mass transfer in bioreactor with three-phase inverse fluidized bed, Bioprocess Eng., 23 (2000) 427-429.

[16] S.W. Kim, H.T. Kim, P.S. Song, Y. Kang, Liquid dispersion and gas-liquid mass transfer three-phase inverse fluidized beds, Can. J. Chem. Eng., 81 (2003) 621-625.

[17] I. Hamdad, S. Hashemi, D. Rossi, A. Macchi, Oxygen transfer and hydrodynamics in three-phase inverse fluidized beds, Chem. Eng. Sci., 62 (2007) 7399-7405.

[18] Y.J. Cho, H.Y. Park, S.W. Kim, Y. Kang, S.D. Kim, Heat transfer and hydrodynamics in two- and three-phase inverse fluidized beds, Ind. Eng. Chem. Res., 41 (2002) 2058-2063.

[19] S.M. Son, K.I. Lee, S.H. Kang, Y. Kang, S.D. Kim, Heat transfer coefficient in viscous three-phase inverse fluidized beds, AIChE J., 53 (2007) 3011-3016.

[20] S. Kumar, L.S. Fan, Heat-transfer characteristics in viscous gas-liquid and gas-liquid-solid systems, AIChE J., 40 (1994) 745-755.

[21] H. Li, A. Prakash, Analysis of bubble dynamics and local hydrodynamics based on instantaneous heat transfer measurements in a slurry bubble column, Chem. Eng. Sci., 54 (1999) 5265-5271.

[22] A.K. Jhawar, A. Prakash, Analysis of local heat transfer and hydrodynamics in a bubble column using fast response probes, Chem. Eng. Sci. 62(24) (2007) 7274-7281.

[23] P. Wilkinson, A. Spek, L. van Dierendonck, Design parameters estimation for scale-up of high-pressure bubble columns, AIChE J., 38 (1992) 544-554.

[24] T.J. Lin, C. Hung-Tzu, Effects of macroscopic hydrodynamics on heat transfer in a three-phase fluidized bed, Catal. Today, 79-80 (2003) 159-167.

[25] H. Li, A. Prakash, Survey of heat transfer mechanisms in a slurry bubble column, Can. J. Chem. Eng., 79 (2001) 717-725.

[26] A. Behkish, R. Lemoine, R. Oukaci, B.I. Morsi, Novel correlations for gas holdup in large-scale slurry bubble column reactors operating under elevated pressures and temperatures, Chem. Eng. J., 115 (2006) 157-171.

Chapter 3 - Synthesis of CO_2 hydrates in a slurry bubble column

Denis Myre, Arturo Macchi*

Department of Chemical and Biological Engineering, University of Ottawa,

161 Louis Pasteur, Ottawa, Ontario, Canada K1N 6N5

Phillip Servio

Department of Chemical Engineering, McGill University,

3610 University Street, Montreal, Québec, Canada H3A 2B2

To be submitted to the 7th International Conference on Gas Hydrates,

Edinburgh, Scotland, 2011.

Abstract

Carbon dioxide hydrates were synthesized in a 0.10m I.D. and 1.22m tall bubble column at temperatures near 4ºC. A cooling jacket was used for heat removal during the exothermic formation of hydrates. Visual observations at different driving forces (pressure lying between 2.75 and 3.60 MPa) were recorded with a digital camera through sight glass. The rate of hydrate formation was strongly dependent on the path used to obtain the desired temperatures and pressures. Pressurizing the system followed by cooling resulted in the formation of CO_2 hydrates when restarting the gas flow. At low gas velocity, the hydrate growth was limited by mass transfer likely due to the formation of a hydrate shell around small bubbles. Clusters of hydrate flakes with entrapped tiny CO_2 bubbles were observed when operating near the Liquid-Hydrate-Vapour equilibrium line at low gas velocities. At higher pressures, denser slurry was seen, particularly when CO_2 condensation partially occurred. At high gas velocities and low temperature, the rate of hydrate formation was limited by the rate of heat removal rather than the mass transfer.

3.1 Introduction

Gas hydrates are non-stoichiometric ice-like compounds composed of water and gas molecules. Under certain thermodynamic conditions, hydrogen bonding between water molecules forms a network that includes cavities (or cages) in which gas molecules (guest molecules) can be trapped. Depending on the composition of the gas and the nature of gas molecules, this structure occurs at relatively high pressures and temperatures slightly above freezing point of water and is stabilized by the presence of the guest molecules (Sloan et al., 2008).

In the past, hydrates were mainly seen as a problem in the oil and gas industry by causing blockages of flow lines. This problem is now partly resolved by the use of hydrate inhibitors. Currently, hydrates are perceived as an alternative for transportation and storage of natural gas, as well as a potential avenue for carbon dioxide capture and its sequestration in deep oceans (Sloan et al., 2008). One of the advantages of gas hydrates would be their self-preservation that would allow storage under less intensive conditions compared to conventional methods (i.e., liquefied natural gas, compressed natural gas) (Giavarini et al., 2004). But this phenomenon is still controversial and needs further research to be confirmed (Mori, 2003).

The choice of the best reactor to produce gas hydrate is still unknown (Linga et al., 2010). Several methods were suggested where the processes can be continuous or semi-batch wise while the dispersed phase can either be the liquid or the gas (Mori, 2003). The advantage of having the gas as the dispersed phase is the possibility of enhancing the gas-liquid mass transfer by bubbling gas into the liquid phase. Furthermore, because the formation of hydrate is an exothermic process, from a heat removal point of view, the method involving the gas as the dispersed phase is preferred since liquid water has a greater heat capacity than gas (Hashemi et al., 2009a).

Many types of reactor having the gas as the dispersed phase were tested to produce gas hydrates. Those includes the continuous flow reactor (Yang et al., 2008), the stirred tank reactor (Bergeron and Servio, 2010; Clarke and Bishnoi, 2005), the equilibrium cell with porous silica gel (Seo, 2005), the kenics-type static mixer (Tajima et al., 2004) and the gas inducing impeller (Linga et al., 2010).

On the other hand, the bubble column was less investigated. Luo et al (2007) produced methane-THF hydrates in a small bubble column (column diameter=25.4 mm, gas superficial velocity from 2 to 10 mm/s) at pressures between 0.4 and 0.8 MPa. However, the low fluid turbulence led to the formation of a shell at the surface of the bubble, which reduced the rate of hydrate formations. Enhanced turbulence at greater gas velocities should reduce or prevent the formation of a shell at the surface of the bubbles, increasing the rate of gas consumption. Hence in this study, carbon dioxide hydrates were produced in a bubble column and the gas consumption was calculated over at greater superficial gas velocities of 20 to 50 mm/s.

3.2 Experimental procedure

3.2.1 Apparatus

Experiments were performed in a SS316 column with an inner diameter of 0.1 m and a maximum liquid level of 1.22 m. The experimental setup is shown in Figure 3.1. Two glass windows of 118.8 mm x 15.6 mm are located on the front and rear sides of the column to allow visual observation. The column wall is jacketed and the coolant temperature can be reduced to 263K. National Instruments hardware and software was used for data acquisition.

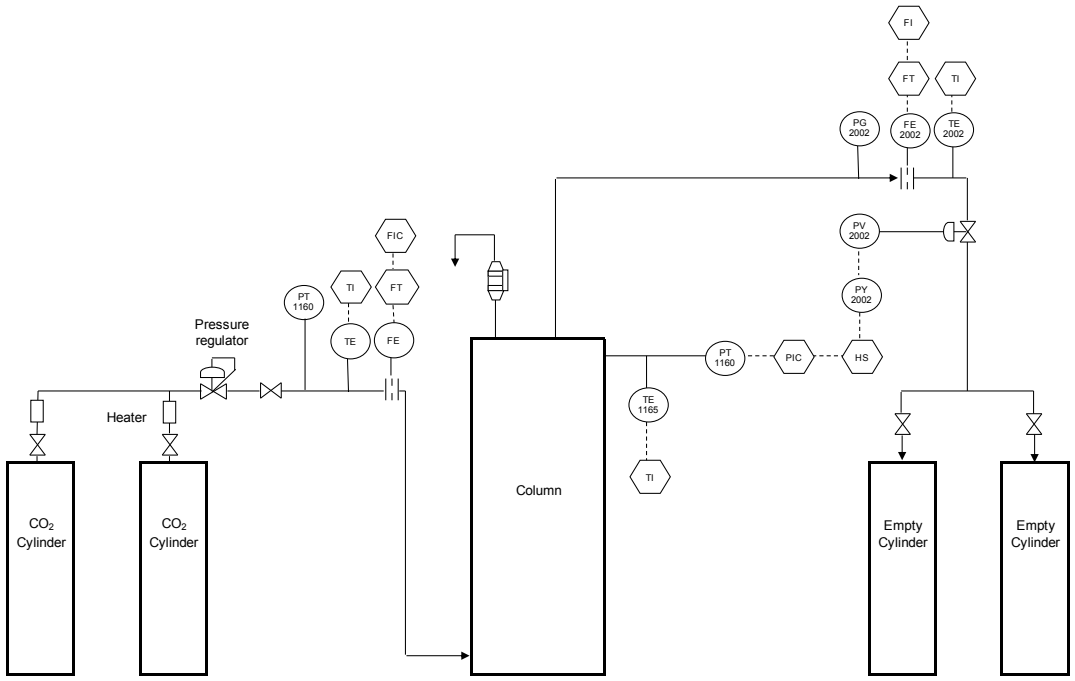

Figure 3.1: Experimental set-up.

The system is adapted to allow a single pass of the gas through the column. A cylinder of carbon dioxide (99.9% purity) feeds the gas at the bottom of the column in which 5000 ml of distilled water was first introduced. The gas passes through a perforated plate with 34 holes of 3.2 mm diameter on a square pattern with a pitch of 15.9 mm for uniformity in gas distribution. The inlet and outlet flow rates are both measured using orifice plates (Rosemount, Model: 1195S010P1S0345CS4J3J1) and pressure transducers (Rosemount, Model: 8732CT12N0). At the column outlet, an automated control valve maintains the system at the desired pressure. At the end, the gas is collected in two empty cylinders.

The gas consumption due to hydrate formation is calculated from temperature, pressure and flow rate measurements before and after the reactor using the Peng/Robinson equation of

state for real gas (Smith et al., 2005). Integrating $\dot{n}_{consumed}$ with respect to time gives the molar quantity of gas consumed during that period of time.

$$\dot{n}_{consumed} = \frac{P_{in}\dot{V}_{in}}{z_{in}RT_{in}} - \frac{P_{out}\dot{V}_{out}}{z_{out}RT_{out}} \quad \ldots(3.1)$$

3.2.2 Procedure

The pressure in the system is increased by flowing gas through the column with the outlet valve closed. Since bubbling gas involves mixing of phases, the sequence used to achieve the desired temperature and pressure conditions influenced the formation of hydrate. The P-T diagram is illustrated on Figure 3.2. In order to produce hydrate, pressure and temperature conditions have to be above the L_w-H-V equilibrium line of the water-carbon dioxide system. In our procedure, the pressure is first increased to the desired value, at a temperature above the three-phase equilibrium temperature. Once desired pressure is attained, the gas flow is reduced to almost zero and the temperature is decreased to the desired value with low mixing of phases by the means of the cooling jacket. Pressure is maintained with the automated outlet control valve. Once the desired pressure and temperature are reached, the flow of gas is restarted with the pressure being maintained. It is to be noted that experiments in which temperature was simultaneously decreased with the increasing pressure resulted in nucleation and growth of hydrate as soon as the L_w-H-V equilibrium line was crossed. Since the reaction is exothermic, heat was generated, the driving force for hydrate growth was limited and the desired temperature was more difficult to attain.

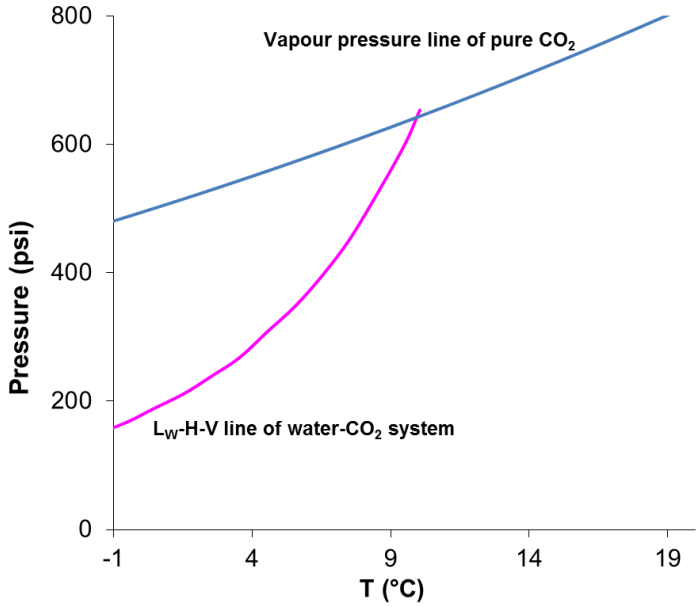

Figure 3.2: P-T diagram showing the vapour pressure line of pure CO_2 and the Lw-H-V line of water-CO_2 system (Sloan et al., 2008).

Each experiment was conducted according to the following sequence:

1) Clean the system with distilled water;

2) Add 5000 ml of distilled water in the column;

3) Purge the system with CO_2 99.9%;

4) Increase pressure to desired value while maintaining the outlet valve closed;

5) Reduce the gas flow to almost zero, and decrease temperature to the desired value via circulating refrigerant fluid;

6) Circulate the gas at desired flow rate and maintain a constant pressure by the action of the automated outlet control valve;

7) Measure the gas consumption and take pictures of the hydrates with a digital camera;

8) At the end, stop the refrigeration system and release the CO_2;

9) Decrease the pressure of the system until gas hydrates decompose completely;

10) Keep the liquid solution for the next experimental run.

3.2.3 Driving forces and operating conditions

The hydrate growth system can be represented by gas bubbles and growing hydrate particles dispersed in the liquid water. Before hydrate formation, for a given pressure, the solubility of CO_2 in liquid water increases with decreasing temperature. Once the L_w-H-V equilibrium line is crossed, the solubility of CO_2 continues to increase but it becomes a "metastable" situation because hydrate formation should be favoured at this point. Figure 3.3 shows the solubility of CO_2 (mol%) as a function of temperature at 3.5 MPa, the dashed line representing the metastable concentration. Initially gas is dissolved into the liquid creating a supersaturated solution relative to H-L_w equilibrium. At the turbidity point, the instantaneous nucleation of hydrate occurs and generates the seed hydrate particles. The formation of seeds consumes the dissolved gas trying to lower the quantity of dissolved CO_2 to the H-L_w equilibrium concentration in the aqueous phase. After the formation of seeds, dissolved gas is utilized for hydrate growth rather than for nucleation. From this point, starting the gas flow involves mass transfer from the gas bubbles to the hydrate particles. Gas molecules thus diffuse across the gas-liquid interface to the liquid bulk in order to compensate the reduction of dissolved CO_2 due to hydrate growth. At the same time, hydrate particles incorporate CO_2 onto their surface trying to lower the bulk CO_2 concentration in order to reach the H-L_w equilibrium concentration.

The gas and liquid phases are assumed to be at equilibrium at the interfaces where the concentration is evaluated at the temperature and pressure of the system. Figure 3.4 shows the concentration, pressure and temperature driving force of the hydrate growth system. The temperature is maximal at the H-L_w interface since reaction is exothermic.

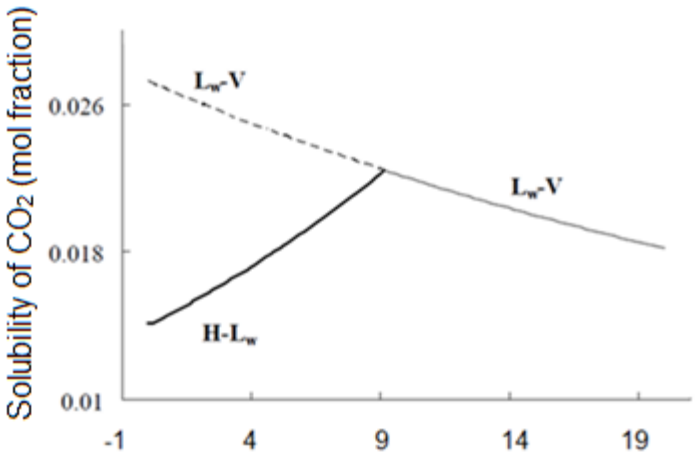

Figure 3.3: Carbon dioxide solubility (mol fraction) in water under liquid water-vapour and liquid water-hydrate equilibrium at P=3.5 MPa (Hashemi et al., 2006).

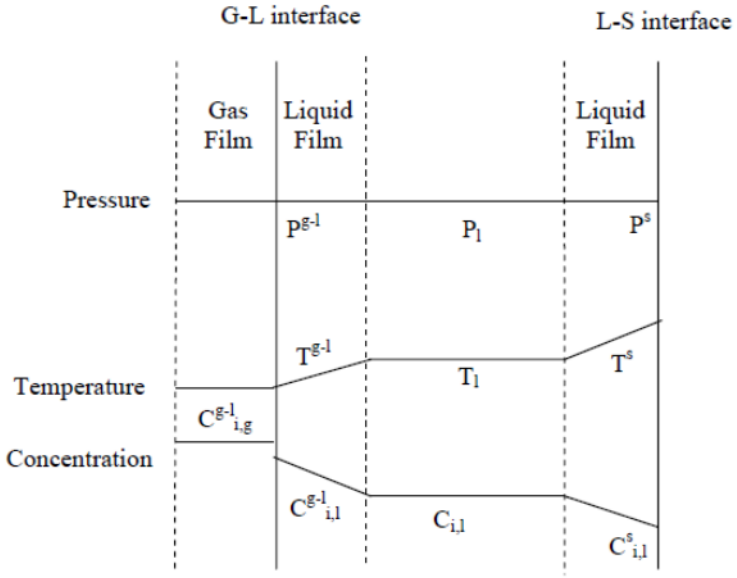

Figure 3.4: Temperature, pressure and concentration driving force within the gas, liquid and solid phases (Hashemi et al., 2009b).

In order to maximize the concentration driving force for hydrate growth, the difference between concentrations of CO_2 at L_w-V and H-L_w equilibrium has to be maximized.

Increasing pressure or decreasing temperature increases this difference with the effect of temperature being more important. Furthermore, because the reaction is exothermic, it is better to decrease the temperature rather than to increase the pressure to distance from the three-phase equilibrium line. In this manner, the temperature difference with equilibrium is greater and the system can absorb more generated heat while remaining in the two-phase H-L_w zone.

In order to prevent the formation of ice in the aqueous phase, the coolant temperature was limited to 0°C and hence the operating temperature was set to 3.5°C in order to maintain a decent temperature driving force for heat exchange.

Different cases for hydrate production were studied. In case 1, it was decided to operate at 3.5°C and 2.75 MPa where the concentration driving force is relatively high. The formation of hydrate was investigated at low superficial gas velocity (20 mm/s) in case 1a and at higher gas velocity (50 mm/s) in case 1b. In case 2, the pressure was raised to 3.6MPa with the temperature remaining at 3.5°C. Because the refrigerant was at 0°C, part of the gaseous CO_2 condensed on the column wall and thus liquid CO_2 droplets were present in aqueous phase. In case 3, hydrates were formed at conditions (2.75MPa and 7.0°C) close to the three-phase equilibrium line. Visual observations were made and explained in terms of transport phenomena.

3.3 Results and discussion

In order to achieve the operating conditions of case 1 (3.5°C and 2.75 MPa), the pressure was increased from atmospheric to 2.75 MPa while temperature was first decreased from room temperature to 10°C. Then, the temperature was decreased to 3.5°C to enter the hydrate zone at very low gas velocity. Once the operating conditions were obtained, the effect of low (Case 1a-20 mm/s) and high gas velocities (Case 1b-50 mm/s) were assessed.

For the low gas velocity case 1a, before starting the gas flow, there was a small quantity of hydrate in aqueous phase (Figure 3.5a) indicating that nucleation and agglomeration already occurred. The hydrate particle size was in the order of 0-0.4 mm. Once the gas flow was started (Figure 3.5b), the bubble flow regime was dispersed with bubble sizes of ~1-2 mm. After few seconds, a thick layer of hydrate surrounding the gas bubbles was observed. The same phenomenon was noted by Luo et al. (2007). Because of the relatively low gas velocity, gas bubbles were small in size with low rise velocities. As a result, the shear stress around the gas bubble is low and the liquid film thickness is considerable. Consequently, the mass transfer coefficient (k_l) within the liquid film is relatively small. As a result, hydrates started to grow at the vapour-liquid interface where the gas concentration is high and formed a shell. The formation of a shell compounded the already poor interphase mass transfer by adding a resistance due to the low diffusivity of CO_2 across the solid hydrate shell. The rate of hydrate growth was thus naturally relatively low. Hydrate growth was accompanied by a slight temperature increase of 0.5°C with a total gas mole consumption of 3% in a period of 6 minutes. When stopping the gas flow (Figure 3.5c), a greater quantity of hydrates particles were observed, with size varying from 0-1 mm.

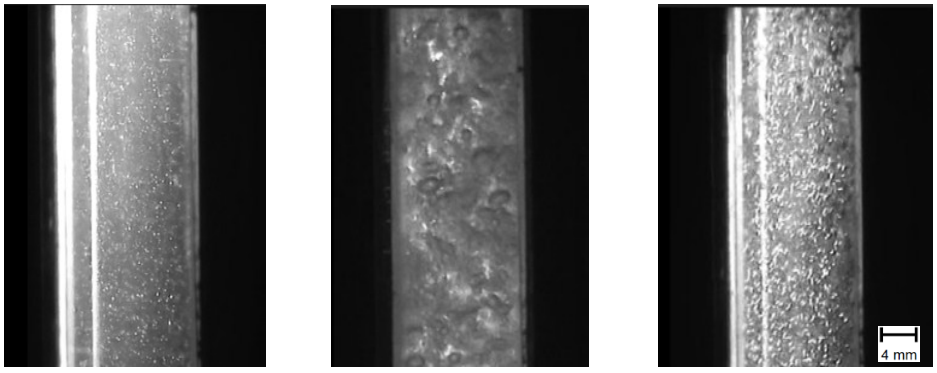

(a) (b) (c)

Figure 3.5: Pictures during hydrate formation at U_g=20 mm/s (P=2.75 MPa, T=3.5°C)

For the high gas velocity case 1b, before starting the gas flow, there was a small quantity of hydrate particle in the aqueous phase (Figure 3.6a) indicating that nucleation and agglomeration already occurred. A few seconds after starting the gas flow (Figure 3.6b), a distribution in bubble sizes was observed (~1 mm to 4 mm). Similarly to the low gas velocity case 1a, gas bubbles were initially surrounded by a hydrate shell and the aqueous solution became visually more opaque and denser. A few seconds later, hydrates started to rapidly (quasi-instantaneously) grow with the vessel being quickly filled with hydrates and large entrapped bubbles (up to 7 mm in size) (Figure 3.6c). The solution became denser and the bubble flow regime changed from dispersed to coalesced because of the high slurry concentration and increased apparent viscosity. At this higher gas velocity, the bubbles were larger with a greater rise velocity. The liquid film thickness around the bubble was thus relatively small due to the greater shear stress, and the hydrate shell around gas bubble did not persist with time. As a result, the mass transfer coefficient ($k_l a$) in the liquid film at the gas-liquid interface was greater as well as the rate of hydrate growth. The sudden large formation of hydrate was accompanied by a temperature increase of 3.5°C with a total gas mole consumption of 17% in a period of 2 minutes. In this case 1b, the hydrate growth was

limited by heat transfer (i.e., heat removal system) rather than interphase mass transfer since the equilibrium temperature at 2.75 MPa was attained rapidly when hydrates started to grow. At the end, when stopping the gas flow (Figure 3.6d), the aqueous phase was filled with hydrates with a few small gas bubbles entrapped.

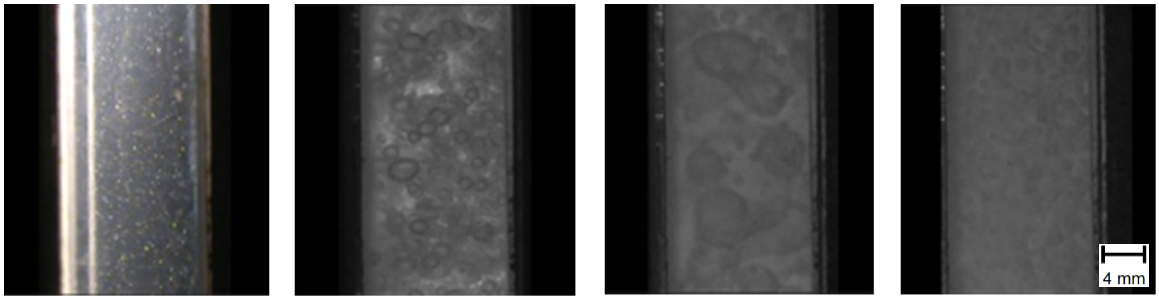

(a) (b) (c) (d)

Figure 3.6: Pictures during hydrate formation at U_g=50 mm/s (P=2.75 MPa, T=3.5°C)

Case 2 (P=3.6 MPa, T=3.5°C, U_g=20 mm/s) where CO_2 partially condensed is illustrated in Figure 3.7. Partial condensation occurred at 3.6 MPa because the wall temperature above the aqueous solution was at 0°C, conditions corresponding to the liquid phase of CO_2. Figure 3.7a shows the water just before CO_2 condensation. A small quantity of hydrates was present in solution indicating that nucleation and agglomeration already occurred. On Figure 3.7b, small opaque CO_2 droplets are observed. As soon as the gas was started, nucleation and then growth occurred immediately (Figure 3.7c). Figure 3.7d shows how concentrated was the hydrate solution at the end of 1 minute of operation, which resulted in a temperature increase of 4.6°C. The presence of liquid CO_2 in the aqueous phase significantly increased the liquid-side volumetric mass transfer coefficient k_la due to the greater diffusivity of liquid CO_2 in water (yielding a greater value of k_l) and due to the lower surface tension of liquid CO_2 in water (yielding smaller droplets and a greater interfacial area).

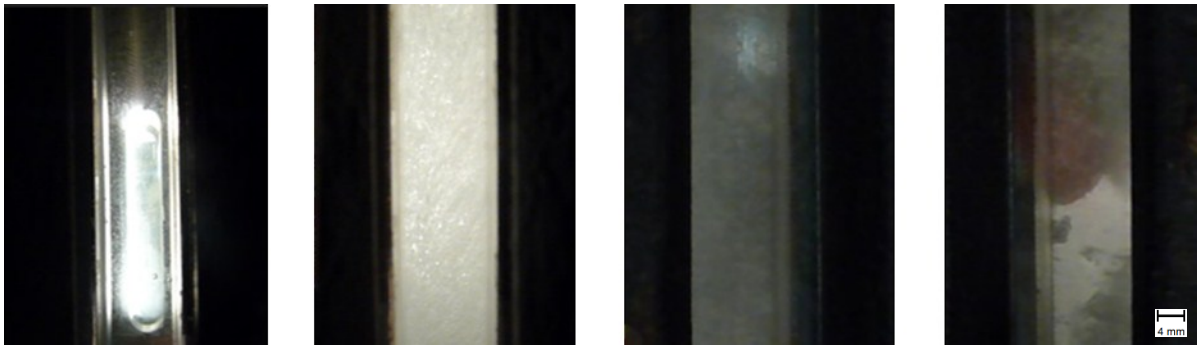

(a) (b) (c) (d)

Figure 3.7: Pictures during hydrate formation at low gas velocity when CO_2 partially condensed (P=3.6 MPa, T=3.5°C)

In case 3 (2.75 MPa and temperature around 7°C), the low driving force region near the L_w-H-V equilibrium line was investigated. At the low gas velocity of 20 mm/s (Figure 3.8 a), a small quantity of hydrate particles was observed several minutes (10 minutes) after entering the hydrate zone, indicating a long induction time. The particles were similar in size to those observed in case 1a, but their quantity and the density of solution was much lower. The small production of hydrates had a minor effect on temperature which continued to decreased (because of cooling system), but at a lower rate. At the larger gas velocity of 50 mm/s (Figure 3.8b), the quantity of hydrate particles increased with the tendency of clustering and entrapping small gas bubbles but the reactor was never filled with hydrates as it was observed at high gas velocity and low temperature (case 1b). The relatively small hydrate growth rate in both cases (non-detectable over a period of 3 minutes) was due the low concentration driving force at conditions close to equilibrium. The pressure was also increased by steps up to 3.4 MPa, resulting in a larger quantity of hydrate particles with greater tendency of agglomerating. But for each pressure step increase, the temperature also increased returning conditions near equilibrium and consequently limiting further hydrate growth.

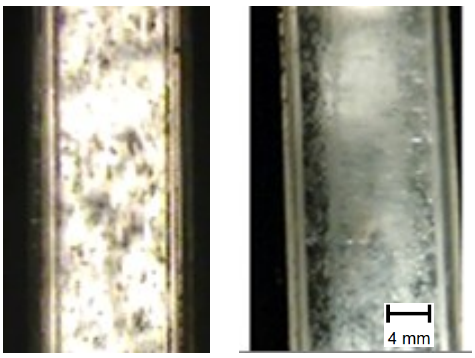

(a) (b)

Figure 3.8: Pictures of hydrate slurry at conditions near the L_w-H-V equilibrium at 2.75 MPa and 7°C.

3.4 Conclusion and recommendations

Gas-Liquid interphase mass transfer and concentration driving force are key factors for hydrate growth. An increase in gas velocity enhances the volumetric mass transfer coefficient k_la while both temperature decrease and pressure increase primarily increase the concentration driving force. At low gas velocity of 20 mm/s (case 1a, case 3a) hydrate growth was limited by poor interphase mass transfer, particularly because of the formation of a hydrate shell around the gas bubble. Case 3a resulted in a lower quantity than case 1a due to the lower concentration driving force. In contrast, at high gas velocity and high concentration driving force (case 1b), the synthesis was limited by heat transfer since the rapid formation of hydrate resulted in a sudden increase of temperature, bringing the condition to L_w-H-V equilibrium. Case 3b did not experience rapid formation of hydrate, although the gas velocity was high, since the concentration driving force was too small. In case 2, the higher pressure increased the k_la value because of condensed CO_2, resulting in the most rapid growth observed even though the gas velocity was small.

In order to maximize hydrate production it is suggested to operate at an intermediary gas velocity to prevent the plugging of the reactor and the sudden temperature increased in the system. Furthermore, it is recommended to continuously remove produced hydrate from the reactor, recuperating the non-reacted water, cool it down and return it back to the reactor in order to reduce the temperature of the system.

Notation

H	Hydrate phase
Lw	Liquid water phase
V	Vapour phase
$\dot{n}_{consumed}$	Rate of CO_2 mole consumption, mol/s
P_{in}, P_{out}	Inlet and outlet pressure, respectively, Pa
$\dot{V}_{in}$, $\dot{V}_{out}$	Inlet and outlet volumetric flow rate of CO_2, respectively, m^3/s
z_{in}, z_{out}	Inlet and outlet compressibility factor of CO_2, respectively, unitless
T_{in}, T_{out}	Inlet and outlet temperature of CO_2, respectively, K
R	Ideal gas constant, $R = 8.314 \frac{Pa \cdot m^3}{mol \cdot K}$

Acknowledgment

The authors are grateful to the *Natural Sciences and Engineering Research Council of Canada* and to *Le Fonds Québécois de la Recherche sur la Nature et les Technologies* for financial assistance.

References

Bergeron, S., Beltrán, J.G., Servio, P., (2010). Reaction rate constant of methane chlatrate formation. Fuel, 89, 294-301.

Clarke, M.A., Bishnoi, P.R., (2005). Determination of the intrinsic kinetics of CO_2 gas hydrate formation using in situ particle size analysis. Chemical Engineering Science, 60, 695-709.

Giavarini, C., Miccioni, F., (2004). Self-perservation at low pressures of methane hydrates with various gas contents. Industrial and engineering chemistry research, 32, 1251-1274.

Hashemi, S., Macchi, A., Servio, P., (2009a). Gas-liquid mass transfer in a slurry bubble column operated at gas hydrate forming conditions. Chemical Engineering Science, 64, 3709-3716.

Hashemi, S., Macchi, A., Servio, P., (2009b). Dynamic simulation of gas hydrate formation in a three-phase slurry reactor. Industrial and Engineering Chemistry Research, 48(15), 6983-6991.

Linga, P., Kumar, R., Lee, J.D., Ripmeester, J., Englezos, P., (2010). A new apparatus to enhance the rate of gas hydrate formation: Application to capture of carbon dioxide. International Journal of Greenhouse Gas Control, 4, 630-637.

Luo, Y.T., Zhu, J.H., Fan, S.S., Chen, G.H., (2007). Study on the kinetics of hydrate formation in a bubble column. Chemical engineering science, 62, 1000-1009.

Mori, Y.H., (2003). Recent advances in hydrate-based technologies for natural gas storage- a review. Journal of chemical industry and engineering. CAS Symposium of gas hydrate, 54.

Seo, Y-T., Moudrakovski, I., Ripmeester, J.A., Lee, J-W., Lee, H., (2005). Efficient recovery of CO2 from flue gas by clathrate hydrate formation in porous silica gels. Environmental Science and Technology, 39, 2315-2319.

Sloan, E.D., Koh, C.A., (2008). Clathrate Hydrates of natural gases. 3rd ed., Boca Raton, FL., CRC Press.

Smith, J.M., Van Ness, H.C., Abbott, M.M., (2005). Introduction to Chemical Engineering Thermodynamics. 7th ed., McGraw-Hill Higher Education.

Tajima, H., Yamasaki, A., Kiyono, F., (2004). Continuous formation of CO_2 hydrate via a kenics-type static mixer. Energy and fuels, 18, 1451-1456.

Yang, D., Le, A., Martinez, R.J., Currier, R.P. Spencer, D.F., Deppe, G., (2008). Heat transfer during CO_2 hydrate formation in a continuous flow reactor. Energy and fuels, 22, 2649-2659.

Chapter 4 - Conclusions and Future Research

4.1 Conclusions

Natural gas hydrates are seen as a potential avenue for transportation and storage of natural gas. The best reactor to produce gas hydrate is still unknown, but the slurry bubble column seems to be promising.

The main motivation of this work was to study the synthesis of carbon dioxide hydrate in a slurry bubble column and observe phenomena that would be similar with natural gas at other conditions. Hence, carbon dioxide hydrates have been synthesized in a bubble column under different operating conditions, and observations were made and analyzed in term of driving forces. Also, since hydrate formation is an exothermic process, it was important to well understand the parameters that affect heat transfer in the reactor. Hence, heat transfer measurements were performed in a natural-gas hydrate simulated environment. As mentioned before, these two objectives were achieved in parallel.

The instantaneous heat transfer measurement gave understanding on bubble dynamics in a gas-liquid-solid system for which the solid phase is less dense than the liquid phase, as it would be the case in a system involving natural gas-water-natural gas hydrate. It was found that an increase in gas and liquid velocities improved the heat transfer coefficient by widening the bubbles size distribution, which directly affects the fluid renewal at the surface of the probe. Also, it was found that low solid loadings have a positive effect on the heat transfer coefficient while larger solid loading tend to lower it due to an increase in the

apparent viscosity of the liquid. It indicates that the presence of hydrates in a large quantity in the bubble column could reduce the capacity of heat removal. On the other hand, the small bubble size in presence of ethanol (to simulate high pressure hydrate system environment) lowered the average heat transfer coefficient due to the poor bubble-induced turbulence.

Gas-to-liquid mass transfer and concentration driving force were found to be key parameters for hydrate growth in a bubble column. An increase in gas velocity enhances the gas-to-liquid mass transfer coefficient while both temperature decrease and pressure increase primarily increase the concentration driving force. For the range of operating conditions investigated, when only one of the key parameters were maximized this led to the slow growth of hydrates, with the rate of mass transfer being the limiting factor. The situation where both concentration driving force and interphase mass transfer were maximized led to the rapid (quasi-instantaneous) formation of CO_2 hydrates, with the reactor being quickly filled with hydrates. In this case, the reaction was limited by heat removal rather than mass transfer.

4.2 Future research

In order to better the production rate of gas hydrates, it is first suggested to improve means for heat transfer. Scaling-up the bubble column with the cooling jacket would further reduce the efficiency of heat removal, suggesting that the cooling jacket is definitely not sufficient. With the present system, one option would be to continuously remove produced hydrate from the reactor, recuperating the non-reacted water, cooling it and returning it back to the reactor, i.e. external means of heat removal as well as control of hydrate population in the reactor.